การไหลที่มีผิวอิสระภายใต้ผลของแรงโน้มถ่วงและแรงตึงผิว เนื่องมาจากการกระจายความดัน

นายมนตรี มาลีวงศ์

วิทยานิพนธ์นี้เป็นส่วนหนึ่งของการศึกษาตามหลักสูตรปริญญาวิทยาศาสตรดุษฎีบัณฑิต
สาขาวิชาคณิตศาสตร์ ภาควิชาคณิตศาสตร์
คณะวิทยาศาสตร์ จุฬาลงกรณ์มหาวิทยาลัย
ปีการศึกษา 2547
ISBN 974-17-6585-1

FREE-SURFACE FLOWS UNDER GRAVITY AND SURFACE TENSION EFFECTS DUE TO PRESSURE DISTRIBUTION

Mr. Montri Maleewong

A Dissertation Submitted in Partial Fulfillment of the Requirements
for the Degree of Doctor of Philosophy in Mathematics

Department of Mathematics
Faculty of Science
Chulalongkorn University

Academic Year 2004
ISBN 974-17-6585-1

Thesis Title	Free-surface flows under gravity and surface tension effects due to pressure distribution
By	Mr. Montri Maleewong
Field of study	Mathematics
Thesis Advisor	Associate Professor Jack Asavanant, Ph.D.
Thesis Co-advisor	Professor Roger Grimshaw, Ph.D.

Accepted by the Faculty of Science, Chulalongkorn University in Partial Fulfillment of the Requirements for the Doctor's Degree

…….. Dean of the Faculty of Science
(Professor Piamsak Menasveta, Ph.D.)

THESIS COMMITTEE

…… Chairman
(Assistant Professor Pornchai Satravaha, Ph.D.)

……Thesis Advisor
(Associate Professor Jack Asavanant, Ph.D.)

……Thesis Co-advisor
(Professor Roger Grimshaw, Ph.D.)

……..Member
(Professor Pramote Dechaumphai, Ph.D.)

…….. Member
(Assistant Professor Ekachai Juntasaro, Ph.D.)

…….. Member
(Assistant Professor Paisan Nakmahachalasint, Ph.D.)

…….. Member
(Assistant Professor Vimolrat Ngamaramvaranggul, Ph.D.)

มนตรี มาลีวงศ์ : การไหลที่มีผิวอิสระภายใต้ผลของแรงโน้มถ่วงและแรงตึงผิวเนื่องมาจากการกระจายความดัน. (FREE-SURFACE FLOWS UNDER GRAVITY AND SURFACE TENSION EFFECTS DUE TO PRESSURE DISTRIBUTION) อ. ที่ปรึกษา : รศ. ดร. จักษ์ อัศวานันท์, อ. ที่ปรึกษาร่วม : Prof. Dr. Roger Grimshaw, 101 หน้า. ISBN 974-17-6585-1

เราพิจารณาการไหลในสองมิติของพื้นผิวอิสระที่เป็นอิสระจากเวลาเนื่องมาจากการกระจายความดัน ภายใต้ผลกระทบของแรงโน้มถ่วงและแรงตึงผิวในน้ำที่มีความลึกคงที่ ของไหลถูกสมมติให้ไม่มีความหนืด ไม่มีการบีบอัดตัว และการไหลเป็นแบบไม่มีการหมุนวน พฤติกรรมของคลื่นไม่เชิงเส้นถูกจำแนกโดยพารามิเตอร์สามตัวคือ Froude number (F) Bond number (τ) และขนาดกับเครื่องหมายของการกระจายความดัน (ϵ) ปัญหาคลื่นไม่เชิงเส้นนี้ ถูกแก้โดยวิธีการเชิงตัวเลขโดยการใช้ระเบียบวิธีการ boundary integral นอกจากนี้เรายังได้ศึกษาทฤษฎีเชิงเส้นและทฤษฎีไม่เชิงเส้นอย่างอ่อนสำหรับในกรณีของคลื่นที่มีความสูงไม่มาก เพื่อหาบทเชื่อมต่อกับคำตอบไม่เชิงเส้น พบว่าเมื่อค่า $\tau > 1/3$ แบบจำลองที่เหมาะสมของทฤษฎีไม่เชิงเส้นอย่างอ่อนคือ สมการ fKdV ขณะที่แบบจำลองที่ดีในกรณีของ $\tau < 1/3$ คือ สมการ fNLS โดยทั่วไปเราพบว่า เมื่อกำหนดค่าของ F และ τ จะเกิดคลื่นที่มีการยกตัวและยุบตัว และในบางกรณี เราพบว่าคำตอบรูปแบบใหม่ของคลื่นไม่เชิงเส้นอยู่ในรูปของคลื่นที่มีหลายโหมด

ภาควิชา	คณิตศาสตร์	ลายมือชื่อนิสิต.....
สาขาวิชา	คณิตศาสตร์	ลายมือชื่ออาจารย์ที่ปรึกษา.....
ปีการศึกษา	2547	ลายมือชื่ออาจารย์ที่ปรึกษาร่วม.....

4373828823 : MAJOR MATHEMATICS

KEY WORD: GRAVITY-CAPILLARY / KdV / NLS / DEPRESSION / ELEVATION WAVE

MONTRI MALEEWONG: FREE-SURFACE FLOWS UNDER GRAVITY AND SURFACE TENSION EFFECTS DUE TO PRESSURE DISTRIBUTION. THESIS ADVISOR: ASSOC. PROF. JACK ASAVANANT, Ph.D., THESIS CO-ADVISOR: PROF. ROGER GRIMSHAW, Ph.D., 101 pp. ISBN 974-17-6585-1

We consider steady two-dimensional free surface flows due to an applied pressure distribution under the effects of both gravity and surface tension in water of a constant depth. The fluid is assumed to be inviscid and incompressible and the flow is irrotational. The behavior of nonlinear waves is characterized by three parameters: the Froude number, F, the Bond number, τ, and the magnitude and sign of the pressure distribution, ϵ. The nonlinear wave problem was solved numerically by a boundary integral method. In addition, we studied some aspects of linear and weakly nonlinear theories in the case of small of amplitude wave to establish connections with the nonlinear solutions. It was found that, when $\tau > 1/3$, the appropriate model for the weakly nonlinear theory is the fKdV equation whereas the fNLS equation gives better description of the wave form solution in the case when $\tau < 1/3$. In general, we found that, when F and τ given, there exist both elevation and depression waves. Also a new family of nonlinear waves in the form of multi-mode waves was demonstrated.

Department	Mathematics	Student's signature……..…..…
Field of study	Mathematics	Advisor's signature……..…..……
Academic year	2004	Co-advisor's signature……..……

ACKNOWLEDGMENTS

First of all, I would like to express great appreciation to my supervisor Assoc. Prof. Dr. Jack Asavanant for his supreme knowledge and guidance within the field of free surface flows. He has been my supervisor over 10 years since I was undergraduate student. All the time, he has always taught me not only academic study but also the way of my life.

My special thanks should be expressed to my thesis co-advisor Prof. Dr. Roger Grimshaw at the Loughborough University, the UK. All the time of my visiting period in the UK (March-September 2004) he constantly gave me very useful suggestions and wonderful ideas especially on the sections of water wave theory. Because of his kindness, I can then complete my work in the parts of linear and weakly nonlinear theories. I would like to thank also the Department of Mathematical Sciences, Loughborough University for their kind support on many facilities, and Prof. Dr. Jean-Marc Vanden-Broeck at the University of East Anglia, the UK for some useful comments on the manuscripts of our papers.

I would particularly like to thank the thesis committee: Prof. Dr. Pramote Dechaumphai, Asst. Prof. Dr. Ekachai Juntasaro, Asst. Prof. Paisan Nakmahachalasint, Asst. Prof. Dr. Pornchai Satravaha, and Asst. Prof. Dr. Vimolrat Ngamaramvaranggul. They kindly read the thesis and offered many useful suggestions on the suitability of the thesis content.

I am also grateful to the Thailand Research Fund through the Royal Golden Jubilee Ph.D. Program for the funding that I received for doing research in Thailand and the UK.

More than 12 years of my study at the Department of Mathematics, Chulalongkorn University, I feel very thankful to my department and all of my teachers who have taught me knowledge and skills. Thank also goes to all of my friends who have always encouraged me until I finished the course of study.

Finally, I feel very grateful to my parents, who have brought me up, standed by me and given me extremely valuable advice.

CONTENTS

NOMENCLATURE

A	amplitude of a wave packet with oscillation wave number k
c	phase velocity
c_g	group velocity
E	mesh spacing
ϵ	magnitude and sign of pressure distribution
η	free surface elevation
$\eta(0)$	value of η at $x = 0$
F	Froude number
F_m	critical value of Froude number at $k = k_m$
g	acceleration of gravity
H	fluid depth at the rest state
k	wave number
k_m	critical value of wave number
λ	wave length; coefficient in the NLS equation
M	number of mesh point
ν_m	critical value of coefficient in the NLS equation
ω	wave frequency
ω_m	critical value of ω
$p(x)$	pressure distribution
p_m	Fourier transform of $p(x)$ at $k = k_m$
p_0	area under the curve $p(x)$
ϕ	potential function
ρ	fluid density
T	coefficient of surface tension
τ	Bond number
U	uniform velocity on the far field upstream
x	spatial coordinate
y	spatial coordinate
$y(0)$	value of y at $\phi = 0$

CHAPTER I

INTRODUCTION

Free surface flow due to an applied pressure distribution in the presence of a uniform stream has been a much-studied problem for more than a century, with applications to the forcing of water waves by atmospheric disturbances, or due to moving obstacles such as ships.

For the two-dimensional flow of an inviscid and incompressible fluid, the key parameters describing the waves are the Froude number $F = U/(gH)^{1/2}$ and the Bond number $\tau = T/\rho g H^2$ where U is the velocity of the uniform stream, H is the undisturbed water depth, ρ is the water density and T is the coefficient of surface tension. To these we add ϵ representing the magnitude and sign of the applied pressure forcing term.

The earliest works, e.g. Rayleigh (1883) used the linearized theory obtained by neglecting nonlinear terms in the free surface boundary conditions. Importantly, the linearized theory reveals that in order to obtain localized solutions it is necessary that $F < 1$ when $\tau > 1/3$, or that $F < F_m < 1$ when $\tau < 1/3$, here F_m is that critical value for which the phase and group velocities coincide at a finite non-zero wavenumber (a formal definition is given in Chapter 2). In Chapters 4 and 6 we confine our attention to the surface-tension dominated case when $\tau > 1/3$, whereas the gravity-dominated case when $\tau < 1/3$ will be considered in Chapters 5 and 7.

The analysis from linear and weakly nonlinear theories reveals that the flow behaviour changes when the critical value $\tau = 1/3$ is passed. That is, for $\tau > 1/3$,

the solutions take the form of classical solitary waves. For small amplitudes and very long wavelengths, the appropriate model from the weakly nonlinear theory is the forced Korteweg-de Vries equation, whose unforced solitary wave solution has the well-known "sech^2" -profile. The connection between these and the fully nonlinear results is discussed in Chapter 6. In contrast, when $\tau < 1/3$, the problem is more complicated than that of the previous case. Now small-amplitude solutions take the form of envelope solitary waves, that is, localized wave packets, and the relevant weakly nonlinear model is the fNLS equation (see Akylas (1993) for the case of zero surface tension, $\tau = 0$).

Nowadays, the fully nonlinear problem can be solved by the use of an accurate numerical method. For instance, Hunter and Vanden-Broeck (1983) used a boundary integral equation method to construct unforced (i.e. $\epsilon = 0$) gravity-capillary waves in water of finite depth problem. They found that depression solitary waves exist when $\tau > 1/3$ and $F < 1$. Their results were consistent with the weakly nonlinear theory associated with the Korteweg-de Vries equation. Recently, accurate fully nonlinear solutions were obtained numerically by Vanden-Broeck and Dias (1992) for the forced problem in water of infinite depth. Their solutions were found to be in good agreement with the linearized theory, and thus extended this into the finite-amplitude regime. Latter, Dias, Menasce and Vanden-Broeck (1996) utilized the same method to solve the unforced case for both infinite and finite depth. They found some new families of gravity-capillary waves.

For $\tau > 1/3$, the validity of the linearized theory then requires that not only should the forcing be sufficiently small ($\epsilon \ll 1$), but also that F be bounded away from 1. When both of these criteria fail, a weakly nonlinear long wavelength theory can be constructed which leads to a forced Korteweg-de Vries equation.

In this thesis, we extend the previous numerical results of Hunter and Vanden-

Broeck (1983) and Vanden-Broeck and Dias (1992) in case of $\tau > 1/3$ by applying a localized symmetric surface pressure distribution to generate gravity-capillary waves in water of finite depth. We assume that the solutions are symmetric and that the flow is subcritical. We find that depression waves exist for $\epsilon > 0$ and $\epsilon < 0$. The branch with $\epsilon > 0$ contains both a solution which bifurcates from a uniform stream, and a solution, which bifurcates from the unforced solitary wave solution, while the branch with $\epsilon < 0$ consists only of a bifurcation from the unforced solitary wave. As F approaches zero, the depression wave exhibits the limiting configuration with a trapped bubble (compare with Crapper's exact solution for $F = 0, \epsilon = 0$, see for instance, Longuet-Higgins 1988). Moreover, we also found that the elevation waves exist only for $\epsilon < 0$ that is as a bifurcation from a uniform flow solution.

When $\tau < 1/3$, the validity of the linearized theory then requires that not only should the forcing be sufficiently small ($\epsilon \ll 1$), but also that F be bounded away from F_m. When both of these criteria fail, a weakly nonlinear theory can be constructed which leads to a forced nonlinear Schrödinger equation (fNLS)

Over the past three decades, unforced wave packet structures have attracted much attention. Zakharov (1968) showed that the two-dimensional evolution of water waves in deep water can be described by the nonlinear Schrödinger equation (NLS). Later Hasimoto and Ono (1972) derived this equation to study the stability of two-dimensional gravity waves in water of finite depth. This was then generalized to three-dimensional waves by Davey and Stewartson (1974). Kawahara (1975) included the effects of surface tension for two-dimensional water waves, while the generalization to the three-dimensional case was done by Djordjevic and Redekopp (1977). Recently, Părău and Dias (2000) treated the steady two-dimensional problem of gravity-capillary waves using a dynamical systems approach. They obtained a normal form equivalent to the steady fNLS model. A stability analysis for these

waves in water of infinite depth was investigated by Calvo and Akylas (2002).

In our work, we extend the NLS equation obtained by Kawahara (1975) to the fNLS equation, and we will show that there is good agreement between the results from this fNLS model and our fully nonlinear results in Chapter 7.

In order to formulate the problem, we consider the steady two-dimensional free-surface flow with a localized applied pressure distribution in water of constant depth. The fluid is assumed to be inviscid and incompressible, and the flow is irrotational. The fluid domain is bounded below by a rigid bottom and above by a free surface. We choose Cartesian coordinates with the x-axis along the free surface and the y-axis directed vertically upwards. Gravity is acting in the negative y direction. Surface tension is included in the dynamic boundary condition on the free surface. Far upstream, the flow is assumed to be uniform with constant velocity U and constant depth H.

The problem can be rendered dimensionless by choosing U, H and UH as velocity, length and velocity potential scales respectively. In terms of these dimensionless variables, the equations governing the motion can be written in terms of the velocity potential $\phi(x, y)$, as follows :

$$\phi_{xx} + \phi_{yy} = 0, \quad -\infty < x < \infty, -1 < y < \eta(x) \tag{1.1}$$

$$\phi_y = 0, \quad y = -1 \tag{1.2}$$

$$\phi_y = \phi_x \eta_x, \quad y = \eta(x) \tag{1.3}$$

$$\frac{F^2}{2}(\phi_x^2 + \phi_y^2 - 1) + \eta = \tau \frac{\eta_{xx}}{(1+\eta_x^2)^{3/2}} - \frac{F^2}{2}\epsilon p(x), \quad y = \eta(x) \tag{1.4}$$

Here η is the free surface elevation, $F = U/\sqrt{gH}$ is the Froude number, $\tau = T/\rho g H^2$ is the Bond number and $\epsilon p(x) = 2p_a(x)/\rho U^2$ is the pressure forcing term.

For given values of F and τ, and the applied pressure $\epsilon p(x)$, the velocity potential $\phi(x, y)$ and the free surface elevation $\eta(x)$ are to be determined, subject to the boundary condition that $\phi \to x$ as $x \to \infty$. This completes the formulation.

In this thesis, we assume either that the forcing function has compact support, or that it decays rapidly at infinity. Further, we shall also assume that $p(x)$ is symmetric, monotone, and non-negative ($p(x) = p(-x) \geq 0$ for all x, and $p_x(x) \leq 0$ for $x \geq 0$). A typical compact forcing function is

$$p(x) = \exp\left({x_b}^2/(x^2 - {x_b}^2)\right) \quad \text{for} \quad |x| < x_b\,,$$

while $p(x) = 0$ for $|x| \geq x_b$ where x_b is the span width of the forcing.

Some aspects from the linearized theory are discussed in Chapter 2. We describe the boundary integral method used to solve numerically the fully nonlinear problem in Chapter 3. Numerical results when $\tau > 1/3$ and $< 1/3$ are shown in Chapter 4 and Chapter 5 respectively. The weakly nonlinear theory associated with the forced KdV equation is presented in Chapter 6 and comparisons made with the numerical results. The derivation of fNLS and the connections between fully nonlinear results and fNLS are shown in Chapter 7. Finally, we conclude some discussion in Chapter 8.

CHAPTER II

LINEAR THEORY

Before proceeding to numerical simulations of the fully nonlinear problem, it is instructive to consider the linearized theory. We put $\phi = x + \bar{\phi}(x, y)$, where $\bar{\phi}(x, y)$ is the small perturbation of ϕ. Substituting this into the governing equations (1.1) - (1.4) and linearizing around the uniform stream, we obtain the set of linear governing equations as follows (the bar symbol is omitted),

$$\phi_{xx} + \phi_{yy} = 0, \quad -\infty < x < \infty, -1 < y < 0 \tag{2.1}$$

$$\phi_y = 0, \quad y = -1 \tag{2.2}$$

$$\phi_y = \eta_x, \quad y = 0 \tag{2.3}$$

$$F^2\phi_x + \eta = \tau\eta_{xx} - \frac{F^2}{2}\epsilon p(x), \quad y = 0 \tag{2.4}$$

We define the Fourier transform of ϕ and its inverse transform as

$$\hat{\phi} = \int_{-\infty}^{\infty} \phi \; e^{-ikx} dx, \quad \phi = \frac{1}{2\pi}\int_{-\infty}^{\infty} \hat{\phi} \; e^{ikx} dk$$

respectively, with an analogous definition for η and $\hat{\eta}$ and the pressure forcing term. Here k is the wavenumber defined by $k = 2\pi/\lambda$ where λ is the wavelength. Applying the Fourier transform to the set of linear equations (2.1) - (2.4), we have

$$\hat{\phi}_{yy} - k^2\hat{\phi} = 0, \quad -\infty < x < \infty, -1 < y < 0 \tag{2.5}$$

$$\hat{\phi}_y = 0, \quad y = -1 \tag{2.6}$$

$$\hat{\phi}_y = ik\hat{\eta}, \quad y = 0 \tag{2.7}$$

$$ikF^2\hat{\phi} + \hat{\eta} = -\tau k^2\hat{\eta} - \frac{F^2}{2}\,\epsilon\hat{p}(x), \quad y = 0\,. \tag{2.8}$$

From the continuity equation, the general solution is

$$\hat{\phi} = A(k)e^{ky} + B(k)e^{-ky}.$$

After satisfying the bottom boundary condition (2.6), we find the solution of (2.5) for $\hat{\phi}$ is

$$\hat{\phi} \;= \frac{a(k)\cosh k(y+1)}{\cosh k}.$$

The remaining boundary conditions then yield the Fourier transform $\hat{\eta}$ of the free surface elevation as

$$\hat{\eta} \;= -\frac{F^2}{2}\,\frac{\epsilon\hat{p}}{[(1+\tau k^2) - F^2 k\coth k]}. \tag{2.9}$$

First, we consider unforced waves. For these, the linear dispersion relation for periodic waves is readily obtained by setting $\epsilon = 0$, which from (2.9) can only be satisfied if the denominator in (2.9) is zero, that is

$$F^2 = (1+\tau k^2)\frac{\tanh k}{k}.$$

Now localized solutions to the linear forced problem, or indeed to the fully nonlinear forced problem, are only expected to exist for those values of F^2 such that there is no real wavenumber k for which this dispersion relation can be satisfied. It is then easily shown that this is achieved either for $\tau > 1/3$ with $0 < F^2 < 1$, or for $\tau < 1/3$ with $0 < F^2 < F_m^2 < 1$ where F_m^2 is defined as the value of F^2 at $k = k_m$ where $\frac{dF^2}{dk} = 0$. Then F_m^2, k_m are given parametrically as functions of τ by

$$\begin{aligned} \frac{1+\tau k_m^2}{1-\tau k_m^2} \;&=\; \frac{\sinh 2k_m}{2k_m}\,, \\ F_m^2 \;&=\; (1+\tau k_m^2)\frac{\tanh k_m}{k_m} \;=\; (1-\tau k_m^2)\frac{\sinh^2 k_m}{k_m^2}\,. \end{aligned} \tag{2.10}$$

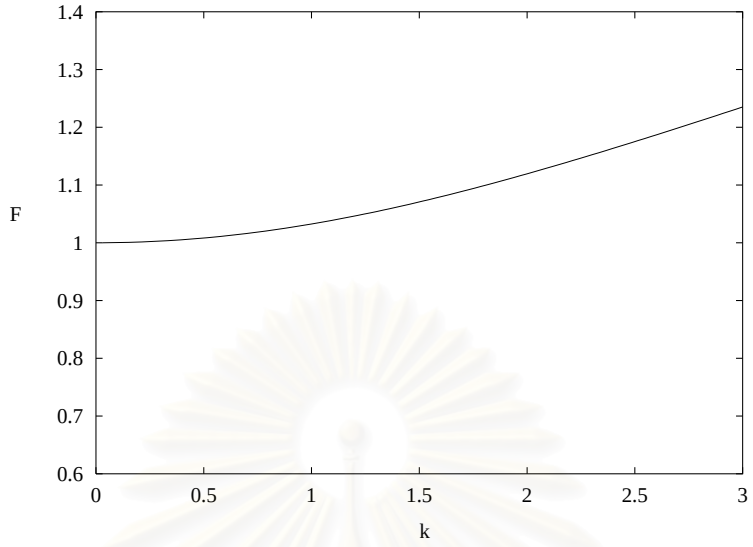

Figure 2.1: Dispersion curve relating F and k when $\tau > 1/3$.

We are now interested in the possible solitary wave bifurcations from the dispersion relation. It is well known that bifurcation phenomenon occurs when the wave speed c equals the group speed c_g or $\frac{dF^2}{dk} = 0$ (Grimshaw and Iooss 2003). There are three possibilities: (i) $k = 0$, (ii) $k = k_m$ for k_m real, and (iii) k_m is a complex number.

(i) When $k = 0$, we have $F^2 = 1$. This yields a long wave solution, namely the "solitary wave". This solitary wave solution bifurcates from the uniform stream at the critical Froude number $F^2 = 1$. Also, these monotonic types of solitary waves exist when $0 < F^2 < 1$ and $\tau > 1/3$. In this case the Korteweg de Vries (KdV) equation is a good prediction to these types of waves for small amplitudes (Hunter and Vanden-Broeck, 1983). Existence of these waves has been proved by Amick and Kirchgässner (1989).

(ii) Here k_m, F_m^2 is determined from (2.10). A bifurcation occurs at the minimum Froude number F_m as shown in Figure 2.2. The solitary wave solutions in this case

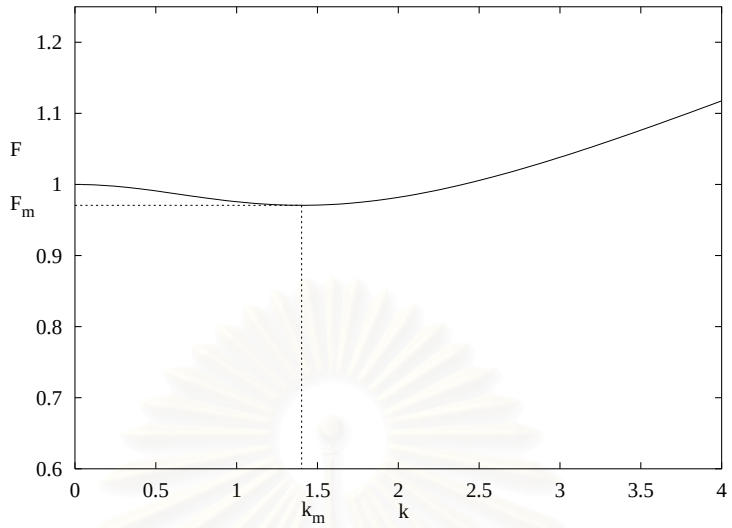

Figure 2.2: Dispersion curve relating F and k when $\tau < 1/3$.

exhibit the form of an envelope wave when $\tau < 1/3$ and $F^2 < F_m^2 < 1$. They have damped oscillations in the tail of the waves. Weakly nonlinear analysis reveals that these solutions are governed by the nonlinear Schrödinger equation (Akylas 1993a). Moreover, the existence of these types of waves has been proved by Iooss and Kirchgässner (1990).

(iii) Another possible bifurcation occurs when $k_m = i\sigma_m$ is a pure imaginary solution of (2.10), i.e.,

$$\frac{1-\tau\sigma_m^2}{1+\tau\sigma_m^2} = \frac{\sin 2\sigma_m}{2\sigma_m},$$

with the corresponding value of F_m^2 obtained from the linear dispersion relation. This bifurcation represents the situation when a solitary wave of finite amplitude changes from a wave with monotonic decay at infinity to one with decaying oscillations at infinity. We will not discuss this case any further here, but see Dias and Iooss (2003) for a more datailed account.

Now we return to the consideration of the forced problem when ϵ is small. Here, we expect the forced solutions to bifurcate either from the uniform stream, or from

the appropriate solitary wave solution. In the former case, the solution is given to leading order by (2.9), while in the latter case the leading order solution will be close to the relevant solitary wave, that is, either the KdV solitary wave if $\tau > 1/3$ or the solitary wave solution of the nonlinear Schrödinger equation if $\tau < 1/3$.

Considering the linearized solution (2.9), let us define $f(k) = (1+\tau k^2) - F^2 k \coth k$. It can be shown that $f(k)$ is always positive whenever F^2 is chosen to ensure the existence of only localized solutions (that is, $0 < F^2 < 1$ for $\tau > 1/3$, and $0 < F^2 < F_m^2$ for $\tau < 1/3$). For a localized forcing function $p(x)$ which is symmetric, monotone and non-negative ($p(x) = p(-x) \geq 0$ for all x, and $p_x(x) \leq 0$ for $x \geq 0$), it can be shown that the Fourier transform $\hat{p}$ is real and positive for all k. Hence, from the definition of the Fourier transform of η, we can infer that η is symmetric and that $\eta < 0 (> 0)$ according as $\epsilon > 0 (< 0)$.

CHAPTER III

NONLINEAR PROBLEM

In this Chapter, we formulate the fully nonlinear problem as an integral equation for the unknown free surface variables by using the boundary integral equation method which is now the standard method to study numerically the potential free surface flow problem. Applications of this method, for example, to various free surface flow problems can be found in Schwartz (1981), Vanden-Broeck and Dias (1992), Asavanant and Vanden-Broeck (1994).

3.1 Formulation

Let us consider the steady two-dimensional irrotational flow of an incompressible inviscid fluid past the applied pressure distribution. Fluid domain is bounded above by the free surface and bounded below by the rigid bottom. A sketch of physical domain plane is shown in Figure 3.1. We include the effects of both gravity g and surface tension T in the dynamic boundary condition on the free surface. Then the Bernoulli equation, in dimensional form, becomes

$$\frac{1}{2}q^2 + gy + \frac{p}{\rho} - \frac{T}{\rho}K = \text{constant on the free-surface} \tag{3.1}$$

where T is the coefficient of surface tension and K is the curvature of the free surface. We define the curvature K by

$$K = \frac{\eta''(x)}{(1+\eta'(x))^{\frac{3}{2}}} \ ,$$

where $\eta(x)$ is the vertical displacment of the free surface measured from the undisturbed water level. We determine the constant on the free surface (3.1) by imposing uniform flow condition at $x = -\infty$. This gives,

$$\frac{1}{2}q^2 + gy + \frac{p}{\rho} - \frac{T}{\rho}K = \frac{1}{2}U^2 + gH + \frac{p_0}{\rho} \, . \tag{3.2}$$

Next, we normalize the problem by choosing H as the length scale and U as the velocity scale. The Bernoulli equation, in dimensionless form, yields

$$F^2q^2 + 2y + F^2\tilde{p} - 2\tau K = 2 + F^2 \tag{3.3}$$

where $\tilde{p} = (p - p_0)/(\frac{1}{2}\rho U^2)$ and $\tau = T/\rho g H^2$. The dimensionless parameter τ is the well known "Bond number" which is the same parameter defined earlier in Chapter 2. In this problem, we restrict our attention in the case of subcritical symmetric flows due to pressure distribution $(F < 1)$. From the assumption of incompressibility and irrotationality, we shall introduce the complex potential $f = \phi + i\psi$ and the complex velocity $w = u - iv$. Without loss of generality, we choose $\phi = 0$ at the intersection point between the free surface and the symmetry line of the compact support forcing function. On the free surface, we set the streamline to be $\psi = 0$. As a consequence, the bottom defines another streamline $\psi = -1$ and the kinematic condition on the bottom is

$$v(\phi, \psi) = 0 \ \text{ on } \ \psi = -1. \tag{3.4}$$

Note that the flow domain in the complex f-plane now is simply an infinite strip (see Figure 3.2).

To obtain the required integral equation, we map the flow domain in the complex f-plane onto the lower half of the complex ζ-plane (See Figure 3.3) by the transfor-

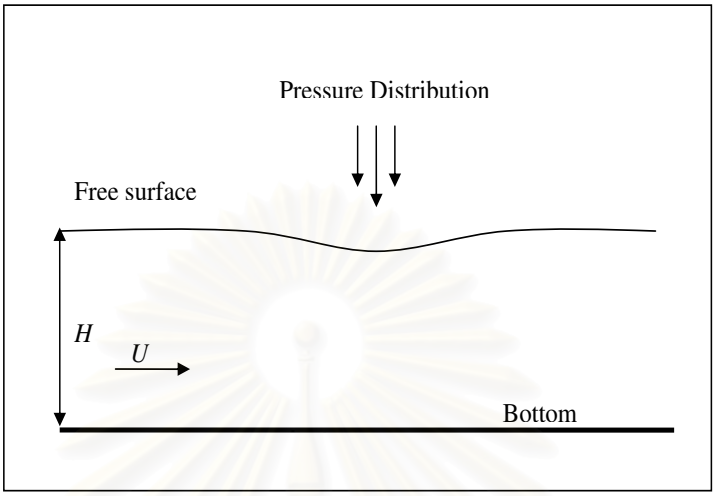

Figure 3.1: Sketch of physical plane.

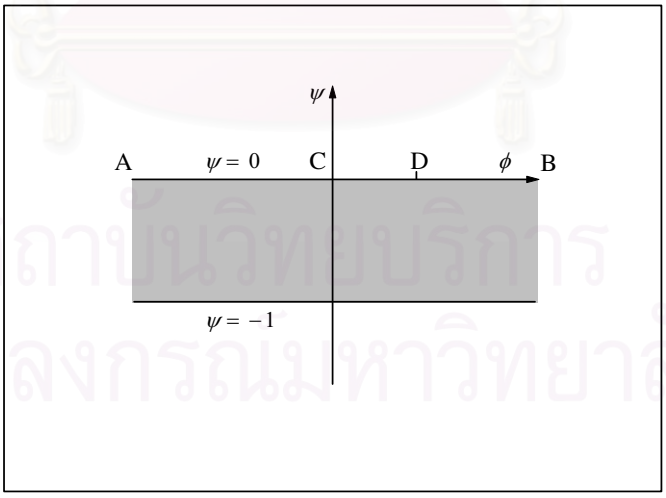

Figure 3.2: Sketch of complex f-plane.

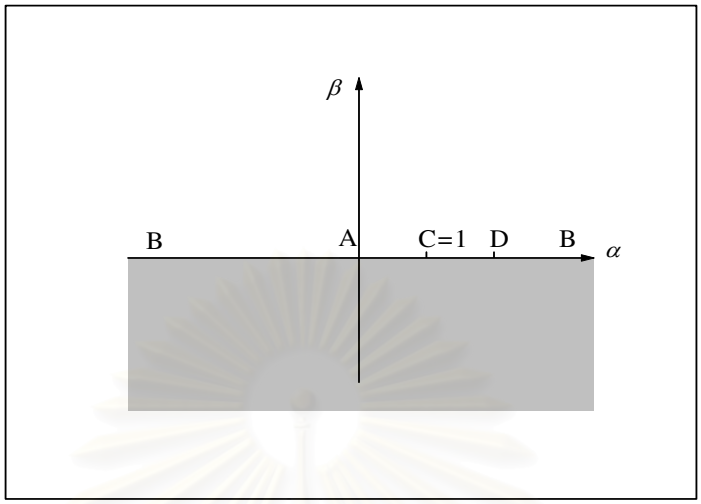

Figure 3.3: Sketch of complex ζ-plane.

mation $\zeta = \alpha + i\beta = \exp(\pi f)$. Instead of using $u(\phi, \psi)$ and $v(\phi, \psi)$, we define w as a function of $\tau'(\alpha, \beta) - i\theta(\alpha, \beta)$ by

$$w = e^{\tau' - i\theta}.$$

In particular, we have the relations $\alpha = e^{\pi\phi}\cos(\pi\psi)$ and $\beta = e^{\pi\phi}\sin(\pi\psi)$. The kinematic boundary condition on the bottom ($\psi = -1$) implies that $\theta(\alpha, 0) = 0$ for $\alpha < 0$. Applying the Cauchy integral formula to the function $\tau' - i\theta$ in the complex ζ-plane where the contour integral is a half-circle oriented in the counter-clockwise direction, we have

$$\tau' - i\theta = -\frac{1}{2\pi i}\oint \frac{\tau'(\zeta') - i\theta(\zeta')}{\zeta' - \zeta}\, d\zeta'.$$

Line integral on the path of half-circle vanishes as we let the radius of the half-circle goes to infinity. Letting ζ approaches the boundary $\beta = 0$, we obtain

$$\tau' - i\theta = -\frac{1}{\pi i}\int_{-\infty}^{\infty} \frac{\tau'(\alpha') - i\theta(\alpha')}{\alpha' - \alpha}\, d\alpha'.$$

After taking the real part, we obtain

$$\tau^{'}(\alpha) = \frac{1}{\pi} \int_{-\infty}^{\infty} \frac{\theta(\alpha')}{\alpha' - \alpha}\, d\alpha' \,. \tag{3.5}$$

The kinematic condition (3.4) imply that

$$\theta(\alpha) = 0 \quad \text{for} \quad \alpha < 0 \,. \tag{3.6}$$

Substituting (3.6) into (3.5), we have

$$\tau^{'}(\alpha) = \frac{1}{\pi} \int_{0}^{\infty} \frac{\theta(\alpha')}{\alpha' - \alpha}\, d\alpha' \,. \tag{3.7}$$

We obtain another relation between $\tau^{'}$ and θ on the free surface by using $w = u - iv = e^{\tau^{'} - i\theta}$. That is $u^2 + v^2 = e^{2\tau^{'}}$. Equation (3.3) then becomes

$$F^2 e^{2\tau^{'}} + 2y + F^2\tilde{p} - 2\tau e^{\tau^{'}} \frac{\partial \theta}{\partial \phi} = 2 + F^2 \,. \tag{3.8}$$

The free surface profile can be determined by integrating numerically the identity

$$\frac{dx}{d\phi} + i\frac{dy}{d\phi} = w^{-1} = \frac{\cos(\theta) + i\sin(\theta)}{e^{\tau^{'}}} \,.$$

That is

$$\frac{dy}{d\phi} = \frac{\sin(\theta)}{e^{\tau^{'}}} \,, \tag{3.9}$$

or

$$\frac{dy}{d\alpha} = \frac{e^{-\tau^{'}} \sin(\theta)}{\pi\alpha} \,. \tag{3.10}$$

Integrating (3.10) yields,

$$y(\alpha) - y(0) = \frac{1}{\pi} \int_{0}^{\alpha} \frac{e^{-\tau^{'}} \sin(\theta)}{\alpha^{'}}\, d\alpha^{'}, \; 0 < \alpha < \infty \,.$$

Since $y \to 1$ as $\alpha \to 0$, we have

$$y(\alpha) = 1 + \frac{1}{\pi} \int_{0}^{\alpha} \frac{e^{-\tau^{'}(\alpha_0)} \sin\theta(\alpha_0)}{\alpha_0}\, d\alpha_0 \,, \; 0 < \alpha_0 < \alpha, \quad \text{as} \quad \alpha \to \infty \,. \tag{3.11}$$

Finally, equations (3.7), (3.8) and (3.11) define a nonlinear integral equation for the unknown function $\theta(\alpha)$ on the free surface. This completes the formulation of our problem.

3.2 Numerical Procedure

We solve the system of integral equations (3.7), (3.8) and (3.11) numerically by placing equally spaced points ϕ_i on $\psi = 0$. The transformation from f-plane to ζ-plane gives

$$\alpha = e^{\pi\phi} \,. \tag{3.12}$$

We write $\tau^*(\phi) = \tau'(e^{\pi\phi})$, $\theta^*(\phi) = \theta(e^{\pi\phi})$ and $y^*(\phi) = y(e^{\pi\phi})$ for brevity. Equation (3.7) then becomes,

$$\tau^*(\phi) = \int_{-\infty}^{\infty} \frac{\theta^*(\phi_0)e^{\pi\phi_0}}{e^{\pi\phi_0} - e^{\pi\phi}} \, d\phi_0 \,. \tag{3.13}$$

Similarly we rewrite (3.8) and (3.11) as

$$F^2 e^{2\tau^*(\phi)} + 2y^*(\phi) + F^2\tilde{p} - 2\tau e^{\tau^*(\phi)} \frac{\partial\theta^*}{\partial\phi} = 2 + F^2 \,, \tag{3.14}$$

$$y^*(\phi) = 1 + \int_{-\infty}^{\phi} e^{-\tau^*(\phi_0)} \sin\theta^*(\phi_0) \, d\phi_0. \tag{3.15}$$

Since we are interested in symmetric subcritical solutions, the following conditions must be imposed

$$\theta^*(-\phi) = -\theta^*(\phi) \quad \text{and} \quad \theta^*(\phi = 0) = 0.$$

Using the above condition, the integral equation (3.13) can be rewritten as

$$\tau^*(\phi) = \int_0^{\infty} \frac{\theta^*(\phi_0)e^{\pi\phi_0}}{e^{\pi\phi_0} - e^{\pi\phi}} \, d\phi_0 - \int_0^{\infty} \frac{\theta^*(\phi_0)e^{-\pi\phi_0}}{e^{-\pi\phi_0} - e^{\pi\phi}} \, d\phi_0 \,. \tag{3.16}$$

Next we introduce the equally spaced mesh points

$$\phi_i = (i-1)E \;,\; i = 1, 2, ..., M$$

where E is the discretization interval. We evaluate the values $\tau_{i+\frac{1}{2}}$ of $\tau^*(\phi)$ in equation (3.16) at the midpoints

$$\phi_{i+\frac{1}{2}} = \frac{\phi_i + \phi_{i+1}}{2} \;,\; i = 1, 2, ..., M-1$$

by using the trapezoidal rule with summation over the points ϕ_i. The symmetry of the quadrature and of the distribution of mesh points enable us to evaluate the integral which is of Cauchy principal value as if it were ordinary integrals (see Appendix). Next we evaluate $y_i = y^*(\phi_i)$ by applying the trapezoidal rule to (3.15). That is,

$$y_M = 1.0 \ ,$$

$$\text{and} \qquad y_{i-1} = y_i - e^{-\tau_{i-\frac{1}{2}}} \sin(\theta_{i-\frac{1}{2}})E \ , \ i = M-1, ..., 1.$$

We then determine $y^*(\phi)$ at the midpoints by using four-points interpolation formula. The free surface condition (3.14) is satisfied by substituting these values of $\tau^*(\phi)$ and $y^*(\phi)$ at the midpoints. This yields $M-1$ nonlinear algebraic equations for the M unknowns $\theta_i, i = 1, ..., M$. The last equation is obtained by imposing the condition

$$\theta_{i-\frac{1}{2}} = 0 \text{ at } \ i = M-1.$$

This system of M nonlinear algebraic equations with M unknowns is solved by Newton's Method.

Let the pressure forcing on the free surface be given by

$$\tilde{P} = \begin{cases} \epsilon \exp\left(\dfrac{1}{(\phi/\phi_B)^2 - 1}\right), & \text{if } \ |\phi| < |\phi_B|; \\ 0, & \text{otherwise.} \end{cases}$$

Note that it is convenient here to specify the pressure forcing in terms of ϕ rather than in terms of x. Thus, except in the linearized limit, the pressure forcing specified here differs from that given at the end of Chapter 1. Of course, once the numerical solution has been obtained, it is straightforward to calculate the form of the pressure forcing as a function of x. For instance, the span length $2x_b$ of the pressure forcing is defined by the integration of $\exp(-\tau')\cos\theta$ over ϕ from $-\phi_B$ to ϕ_B.

For small amplitude solutions it is clear that $x_B \approx \phi_B$; from our numerical results we find that in general x_B increases with ϵ for elevation waves, but decreases with ϵ for depression waves. In this work, we fix $\phi_B = 1.45$ for all calculations.

In the numerical procedure, the integral equation (3.16) must be truncated. Numerical accuracy is tested by varying the number of mesh points M and mesh spacing E. For a fixed $M = 401$, computed profiles for $E = 0.025$ and 0.05 are shown in Figure 3.4. This shows that numerical solutions are insensitive to the mesh spacing when $E \leq 0.05$. On the other hand, Figure 3.5 shows a comparison of computed profiles when $M = 399$ and 699 for a fixed $E = 0.05$. These constitute the sensitivity tests of numerical solutions on M and E. Hence, for the results shown here for the case $\tau > 1/3$, we choose $M = 401$ and $E = 0.05$ in all calculations. In contrast for the case $\tau < 1/3$, more inflexion points appear on the free surface profile and the wave solutions are in form of modulated wave. Then more mesh points are needed to capture the small wave solutions. Thus to keep the desired solution accuracy, we use $M = 699$ and $E = 0.05$ for most of calculations in case of $\tau < 1/3$.

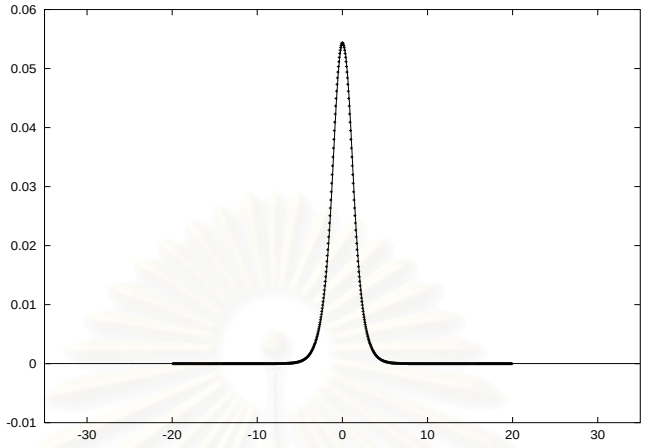

Figure 3.4: Typical free surface profiles for $\tau = 0.4$, $\epsilon = 0.1$ and $F = 0.9$ when $M = 401$. Point represents $E = 0.025$ and solid line represents $E = 0.05$.

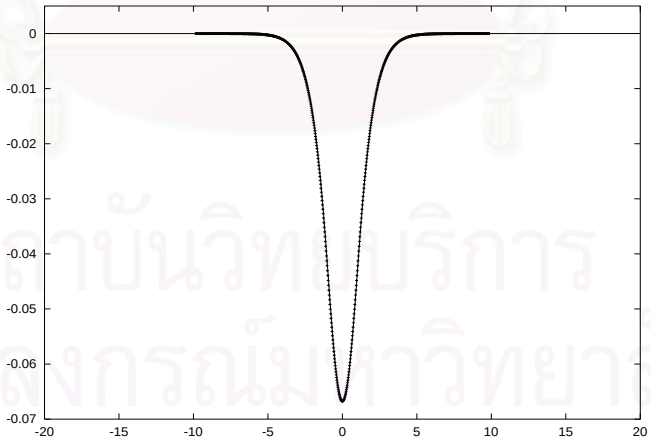

Figure 3.5: Typical free surface profiles for $\tau = 0.4$, $\epsilon = -0.1$ and $F = 0.9327$ when $E = 0.05$. Point represents $M = 399$ and solid line represents $M = 699$.

CHAPTER IV

NUMERICAL RESULTS : BOND NUMBER GREATER THAN ONE-THIRD

In this Chapter, we use the numerical procedure described in the previous Chapter to compute gravity-capillary wave solutions for various values of flow parameters, F and ϵ. We restrict our attention to the case of symmetric subcritical flows when $\tau > 1/3$ and $F < 1$. The case when $\tau < 1/3$ will be considered in the next Chapter.

Hunter and Vanden-Broeck (1983) investigated this problem without any forcing term ($\epsilon = 0$). They found numerically that limiting configuration of depression waves with a trapped bubble exists only when $\tau < 1/2$. From our calculations, this is also the case for depression waves when $\epsilon \neq 0$. We therefore present and discuss numerical results when $\tau = 0.4$ and 0.7 as the other values yield qualitatively similar results for $1/3 < \tau < 1/2$ and $1/2 < \tau$ respectively. Here the unforced solutions $\epsilon = 0$ will be referred to as depression solitary waves or elevation solitary waves.

4.1 Depression wave, $y(0) < 0$

When $\tau = 0.4$, depression wave exists for $\epsilon < 0, > 0$ and $= 0$. Relationship between F and $y(0) < 0$ is shown in Figure 4.1. For each $\epsilon > 0$ branch, there exists critical Froude numbers F_1 and F_2 such that there is a unique solution when $0 < F < F_1$, two solutions when $F_1 < F < F_2$, and no solutions when $F_2 < F < 1$. One family of solutions can be viewed as a perturbation from a uniform stream and the other is a perturbation from a solitary wave. For instance, when $\epsilon = 1.0$ the value of

$F_1 = 0.095$ and $F_2 = 0.7443$. The non-uniqueness of solution at the same value of F is shown in Figure 4.2 when $\epsilon = 5.0$. Note that the vertical axis and horizontal axis shown in Figure 4.2 represent the displacment in vertical and horizontal directions respectively. So, with this understanding, we will obmit label axis in all Figures of free surface profiles presented below in this thesis.

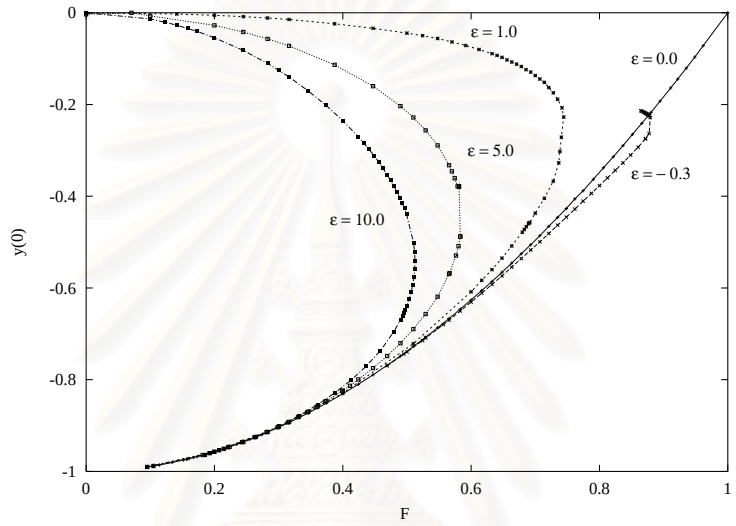

Figure 4.1: Relationship between F and $y(0) < 0$ when $\tau = 0.4$

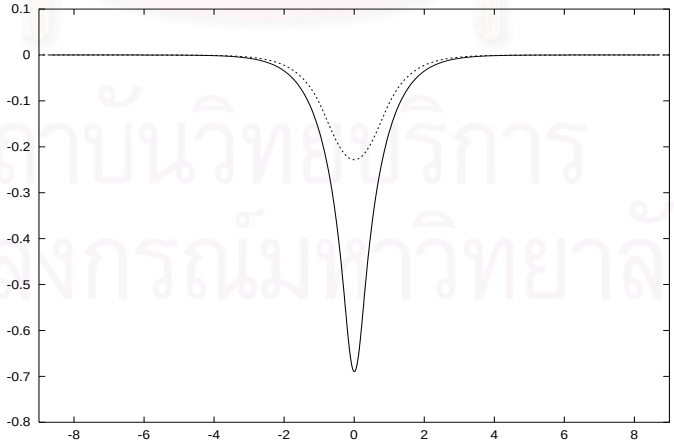

Figure 4.2: Typical free surface profiles for $\tau = 0.4$, $\epsilon = 5.0$ and $F = 0.51$.

As the critical value F_1 is reached, the solution approaches its limiting configuration with a trapped bubble as shown in Figure 4.3. The other critical value F_2 can be viewed as a point at which the solution changes from the bifurcation from a uniform stream to the bifurcation from a solitary wave.

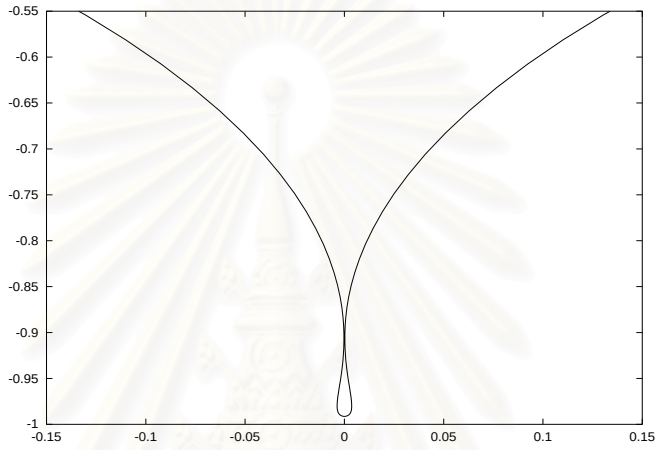

Figure 4.3: Limiting configuration with a trapped bubble for $\tau = 0.4$, $\epsilon = 0.0$ and $F = 0.089$.

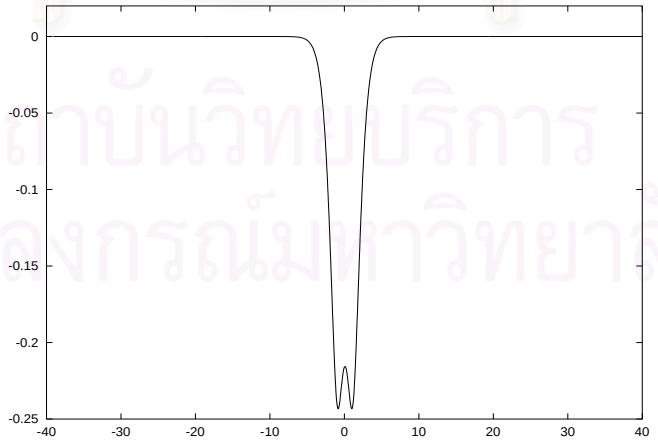

Figure 4.4: Typical free surface profiles for $\tau = 0.4$, $\epsilon = -0.3$ and $F = 0.8678$.

When $\epsilon < 0$ ($\epsilon = -0.3$ in Figure 4.1), there exist depression wave solutions up to a critical Froude number F_3 ($F_3 = 0.8792$, $\epsilon = -0.3$) which is the turning point of this solution branch. After this turning point, the profile of the free surface is dimpled at $y(0)$ (Figure 4.4), and the calculation requires more mesh points ($M = 800$) in order to maintain the desired accuracy. Detailed discussion of this situation is given in chapter 6. But we note here that the existence of this turning point F_3 is an artefact of plotting $y(0)$ rather than the actual minimum value of y_m of $y(x)$ for these dimpled solutions, since $y_m < y(0)$. Of course before the appearance of the dimple, the solutions are monotonic in $x > 0$ and $y_m = y(0)$.

It should be noted that all the solutions found here have a deformed portion of the free surface greater than the forcing width x_B, indicating that the solution structure is mainly determined by the internal dynamics of the fluid rather than directly by the applied pressure forcing; the latter serves mainly to excite the wave, rather than to determine its structure. In general, as ϵ increases, the wave amplitude increases, but the wavelength decreases.

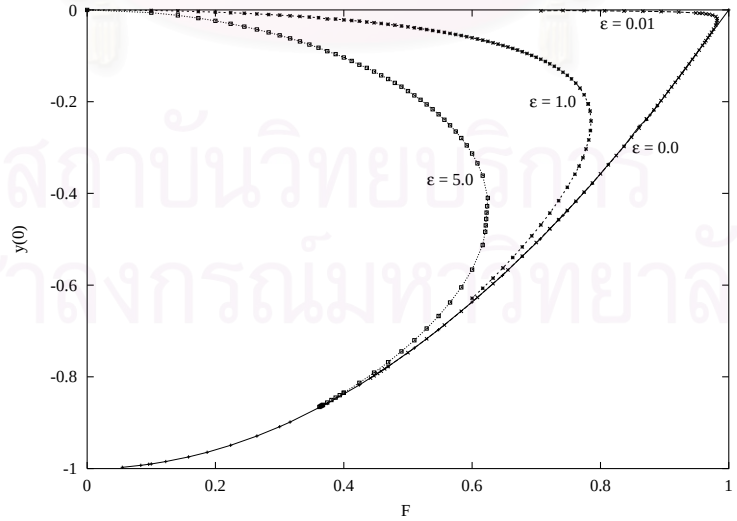

Figure 4.5: Relationship between F and $y(0) < 0$ when $\tau = 0.7$

A similar discussion can be made for the case of $\tau = 0.7$ except for the form of the limiting configuration. The relationship between the Froude number F and the amplitude $y(0) < 0$ for $\epsilon \geq 0$ is shown in Figure 4.5. There are again two critical values, $F_{1,2}$ such that there is a unique solution when $0 < F < F_1$, two solutions when $F_1 < F < F_2$, and no solutions when $F_2 < F < 1$. For instance, when $\epsilon = 1.0$ the value of $F_1 = 0.055$ and $F_2 = 0.7853$. As $F \to F_1$, the solution approaches its limiting configuration, which is now a cusp at $y(0)$ (see Figure 4.6 in case of $\epsilon = 0$) signifying a balance between the gravity and the surface tension terms in the Bernoulli equation. The branch of negative forcing $\epsilon = -0.5$ is shown in Figure 4.7. It is different from the case of $\tau = 0.4$. Although, we apply the pressure distribution with relatively high in magnitude of ϵ, the branch of negative forcing is closely fit to the unforced branch, $\epsilon = 0$.

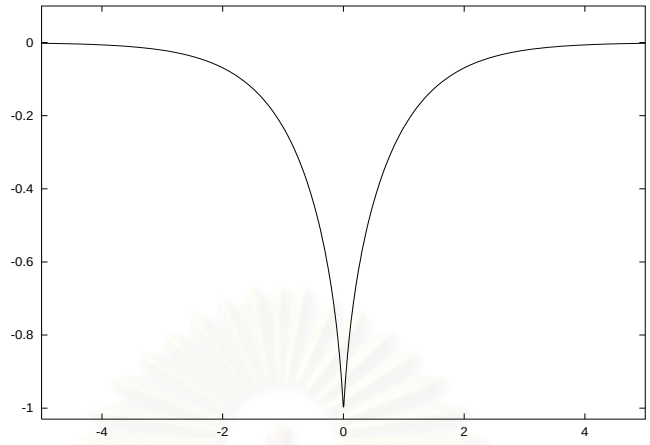

Figure 4.6: Limiting configuration with a cusp at $y(0)$ for $\tau = 0.7$, $\epsilon = 0.0$ and $F = 0.055$

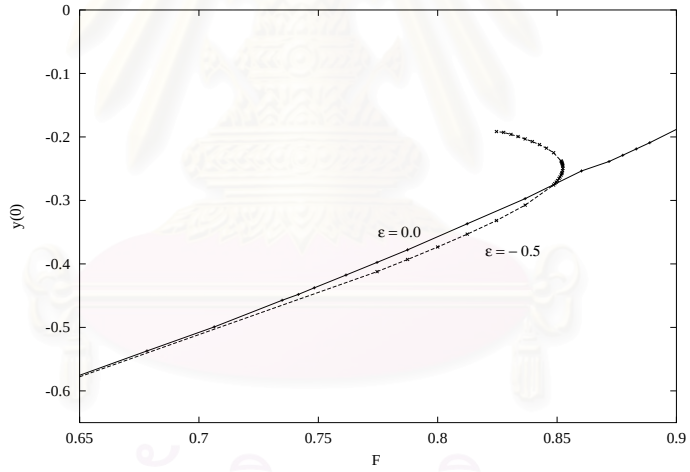

Figure 4.7: Relationship between F and $y(0) < 0$ when $\tau = 0.7$.

4.2 Elevation wave, $y(0) > 0$

We found that the elevation waves exist only when $\epsilon < 0$ and these solutions exist for all the value of Froude number lies between 0 and 1. These are different from the case of depression wave. The solutions are perturbed by the uniform flow solution. The relationship between F and $y(0) > 0$ when $\tau = 0.4$ for various values of $\epsilon < 0$ is shown in Figure 4.8. Typical free surface profiles of elevation waves for $\epsilon = -0.01$ when $F = 0.5$ and 1.0 are shown in Figures 4.9 and 4.10 respectively. We can see that the wavelenght of elevation wave increases as F increases. These numerical results suggest that elevation waves with $\epsilon < 0$ can be extended right up to the critical Froude number $F = 1$.

Finally, we consider the elevation waves in the case of $\tau = 0.7$. The relationship between F and $y(0)$ for various values of $\epsilon < 0$ is shown in Figure 4.11. Typical free surface profile when $F = 1.0$ and $\epsilon = -0.1$ is shown in Figure 4.12. Since the wavelength of elevation wave is very large, the difficulty in our numerical calculation is apparent when the value of $F \to 1$. Thus more mesh points are needed in the computation to maintain the desired accuracy.

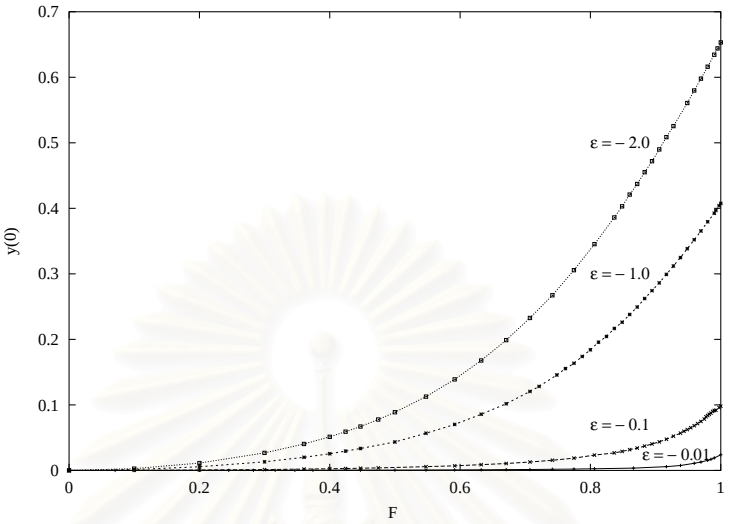

Figure 4.8: Relationship between F and $y(0) > 0$ when $\tau = 0.4$.

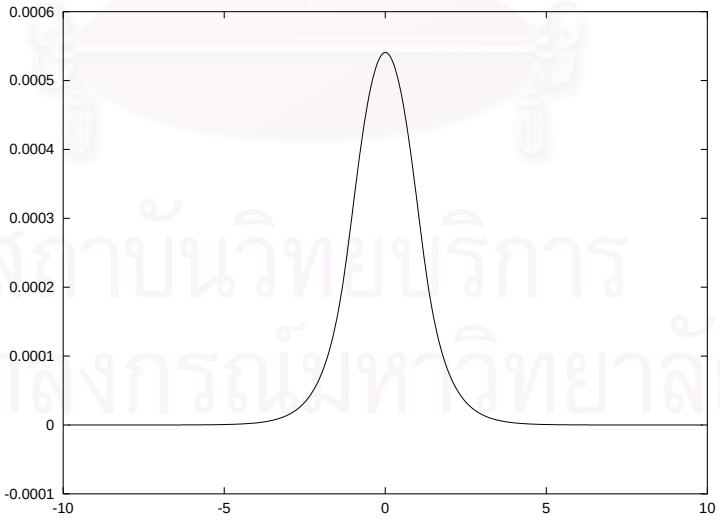

Figure 4.9: Typical free surface profile for $\tau = 0.4$, $\epsilon = -0.01$ and $F = 0.5$

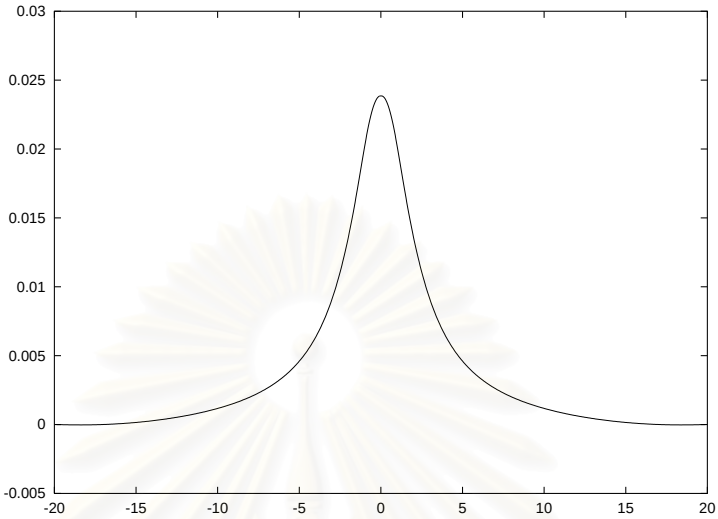

Figure 4.10: Typical free surface profile for $\tau = 0.4$, $\epsilon = -0.01$ and $F = 1.0$

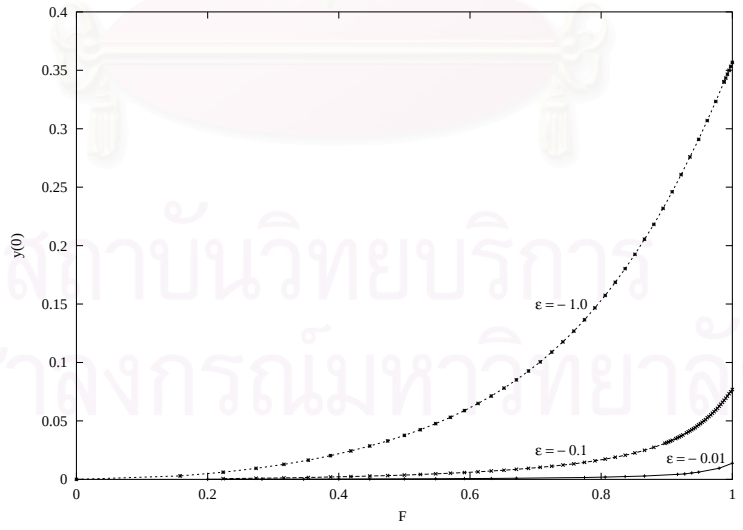

Figure 4.11: Relationship between F and $y(0) > 0$ when $\tau = 0.7$.

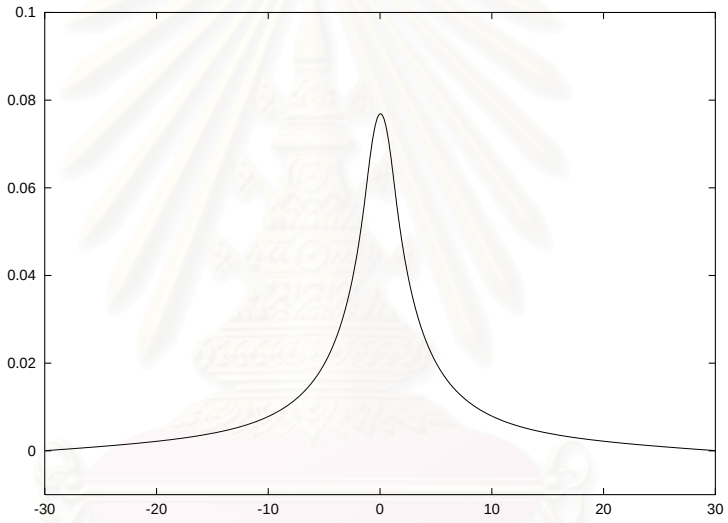

Figure 4.12: Typical free surface profile for $\tau = 0.7$, $\epsilon = -0.1$ and $F = 1.0$

CHAPTER V

NUMERICAL RESULTS : BOND NUMBER LESS THAN ONE-THIRD

In this Chapter, we consider the case of symmetric subcritical flows ($F < F_m < 1$) when $\tau < 1/3$. We present our numerical results when $\tau = 0.25$ for depression and elevation waves (according to $y(0) < 0$ and $y(0) > 0$ respectively). Note that for $\tau = 0.25$, we obtain from equation (2.10) that $F_m = 0.9707$. The case of unforced solutions $\epsilon = 0$ will be referred to as depression solitary waves or elevation solitary waves.

5.1 Depression waves, $y(0) < 0$

It is found that solutions in the form of depression waves can be obtained for both ϵ positive and negative. The relationship between $F < F_m$ and $y(0)$ for various values of ϵ is shown in Figure 5.1.

For each branch of $\epsilon > 0$, there exist critical Froude numbers F_1 and F_2, both dependent on ϵ, such that there is a unique solution when $0 < F < F_1$, two solutions when $F_1 < F < F_2$, and no solutions when $F_2 < F < 1$. One family of solutions can be viewed as a perturbation from a uniform stream and the other is a perturbation from a depression solitary wave. Similar solution behaviors but with different wave profiles can also be found in the case of $\tau > 1/3$. The major difference is that there are more inflexion points on the wave profiles in the present case of $\tau < 1/3$, indicating that these waves resemble wave packets when the amplitude is small. The

nonuniqueness of solution behavior are shown in Figure 5.2 and 5.3 for the same value of F.

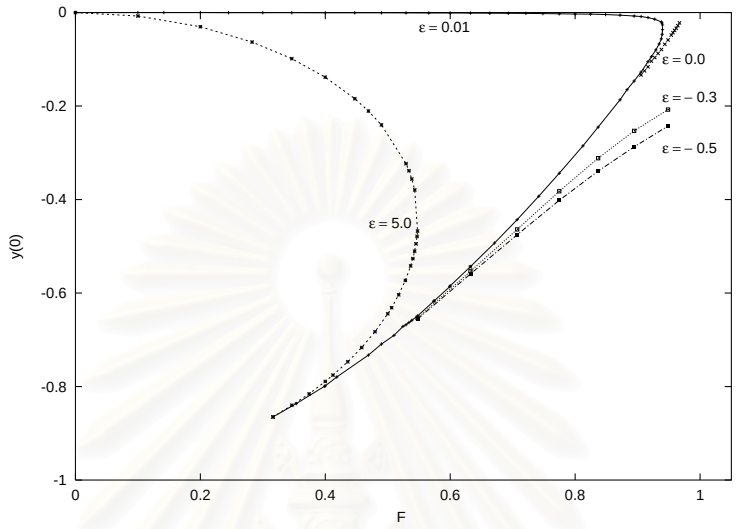

Figure 5.1: Relationship between F and $y(0)$ when $\tau = 0.25$ for various values of ϵ.

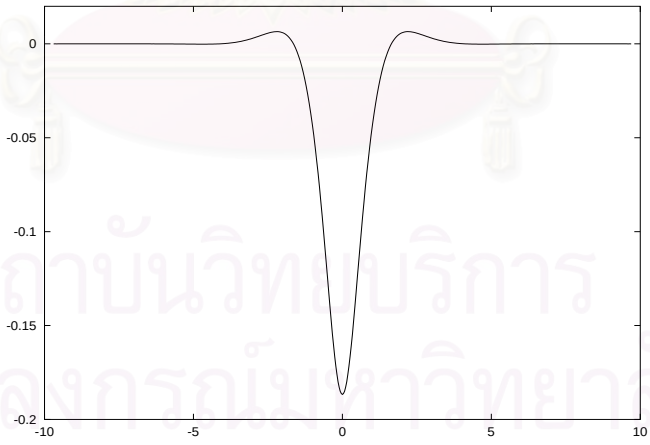

Figure 5.2: Typical free surface profile when $\tau = 0.25$, $F = 0.8717$ and $\epsilon = 0.01$.

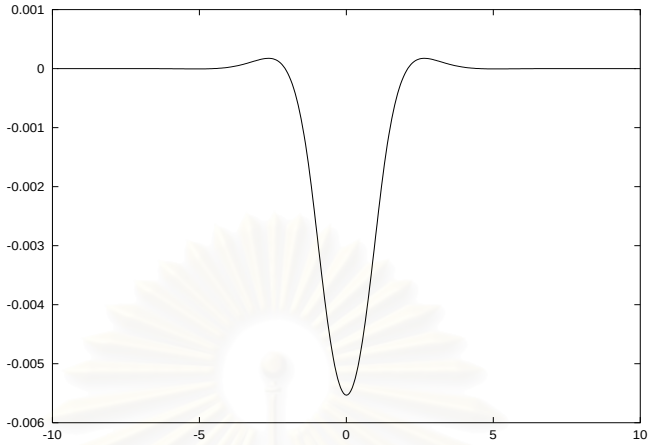

Figure 5.3: Typical free surface profile when $\tau = 0.25$, $F = 0.8717$ and $\epsilon = 0.01$.

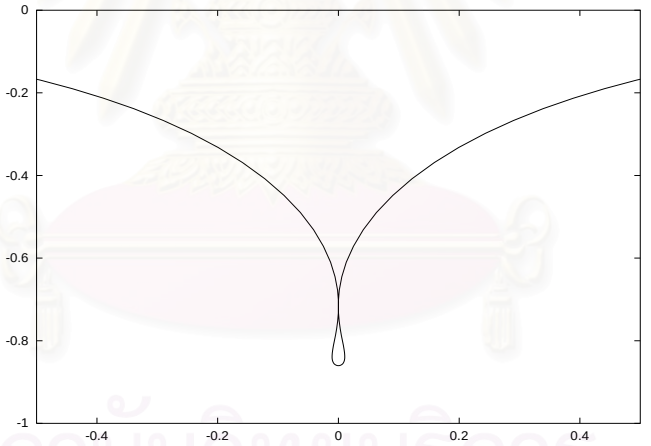

Figure 5.4: Typical free surface profile when $\tau = 0.25$, $F = 0.3245$ and $\epsilon = 0.01$.

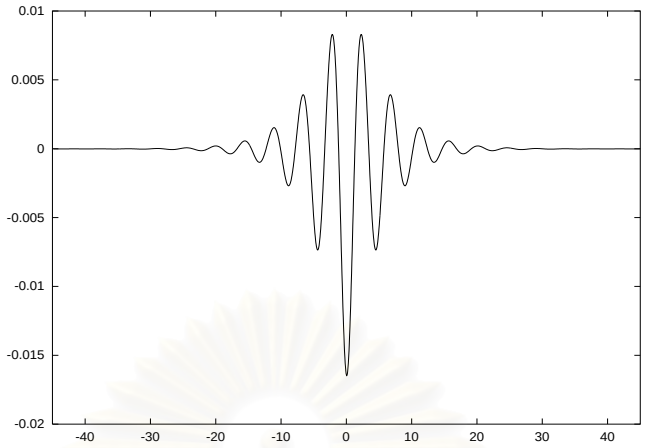

Figure 5.5: Typical free surface profile of enveloped depression solitary wave.

As the critical value of F_1 is reached, the solution approaches its limiting configuration with a trapped bubble as shown in Figure 5.4. This type of solutions in the case of unforced wave was previously found by Hunter and Vanden-Broeck (1983), and Longuet-Higgins (1988).

For $\epsilon = 0$, a branch of depression solitary waves exists in the range $F_1 < F < F_m$. As F approaches F_m, there are more inflexion points on the free surface and the wave profile takes the form of an envelope solitary wave. That is a wave package (see Figure 5.5). The weakly nonlinear model associated with the NLS equation reveals the existence of these solutions (Akylas (1993)). We will defer the comparisons between our nonlinear and the weakly nonlinear model to Chapter 7.

Due to the occurrence of inflexion points on the free surface when F is close to F_m, the computation requires more mesh points in order to get the desired solution accuracy. Thus, computing solutions in the limit $F \to F_m$ becomes increasingly difficult.

When $\epsilon < 0$, there exists a unique solution of depression waves that bifurcate from $\epsilon = 0$ for $F_1 < F < F_m$ as shown in Figure 5.1. The limiting configuration

with a trapped bubble occurs when $F \to F_1$. As F increases, the depression wave develops more inflexion points whereas the wavelength increases. The calculations again become formidable as F approaches F_m. Typical free surface profiles for $\epsilon = -0.5$ and $F = 0.7071$ and 0.8945 are shown in Figure 5.6 and 5.7 respectively.

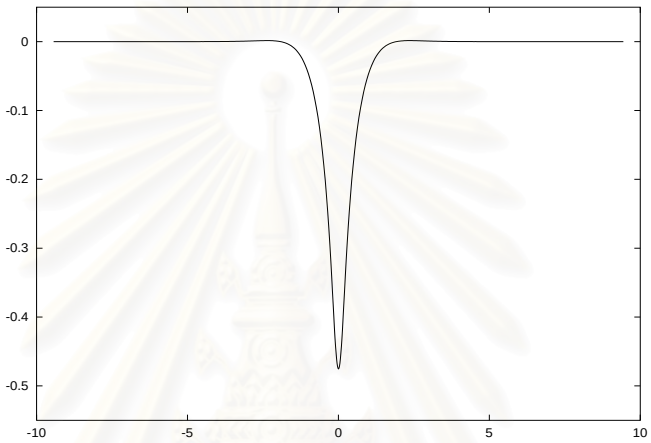

Figure 5.6: Typical free surface profile when $\tau = 0.25$, $F = 0.7071$ and $\epsilon = -0.5$.

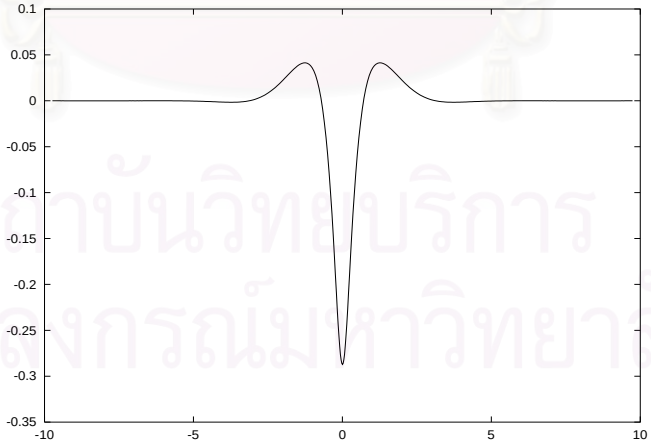

Figure 5.7: Typical free surface profile when $\tau = 0.25$, $F = 0.8945$ and $\epsilon = -0.5$.

5.2 Elevation waves, $y(0) > 0$

Similar to the case of depression waves, there are elevation wave solutions for both ϵ positive and negative. The relationship between F and $y(0)$ for various values of $\epsilon < 0$ is shown in Figure 5.8. The blow up of the turning point of the $\epsilon = 0$ and -0.01 branches is shown in Figure 5.9. Similar behaviour is also found in the case of very small $\epsilon > 0$ which we will discuss further in chapter 7.

For the $\epsilon < 0$ branch, there exist critical Froude numbers F_3 and F_4, again dependent on ϵ, such that there is a unique solution when $0 < F < F_3$, two solutions when $F_3 < F < F_4$, and no solutions when $F_4 < F < F_m$. One family of solutions can be viewed as a perturbation from a uniform stream and the other is a perturbation from a solitary wave. These results differ from the case of $\tau > 1/3$ in that only the perturbation solution from uniform stream can be found for $0 < F \leq 1$.

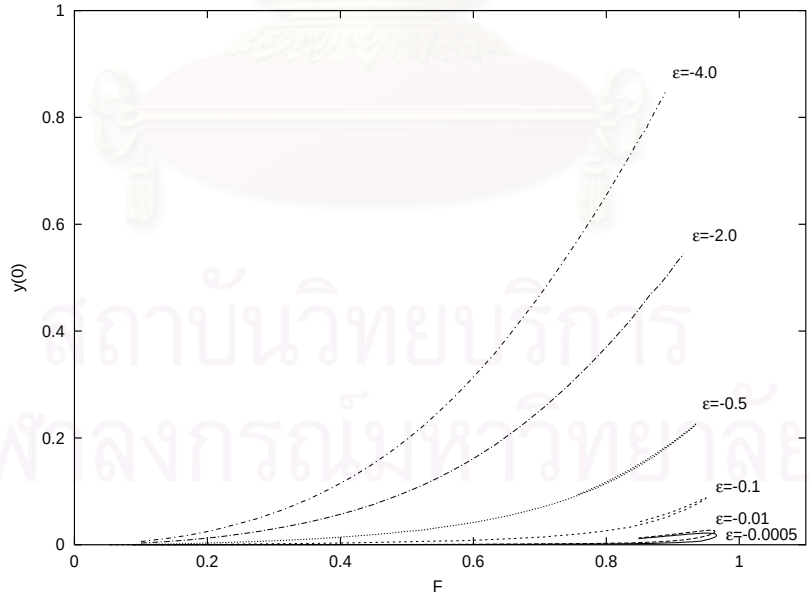

Figure 5.8: Relationship between F and $y(0)$ when $\tau = 0.25$ for various values of $\epsilon < 0$.

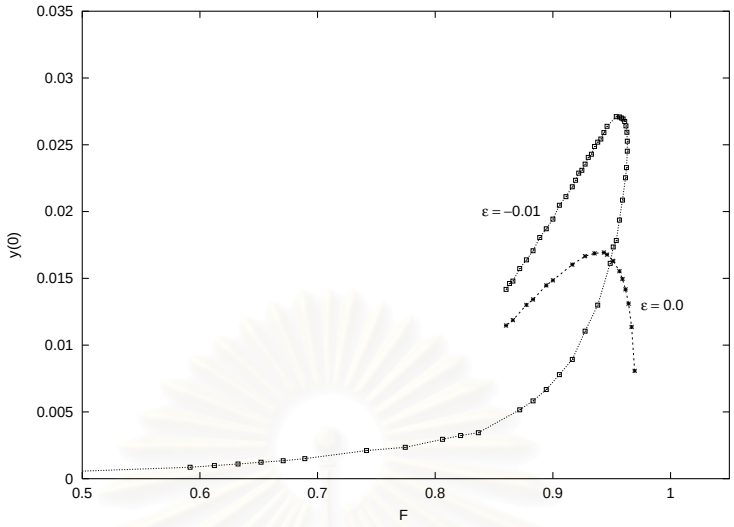

Figure 5.9: Blow up of the solution branches for $\epsilon = 0.0$ and -0.01.

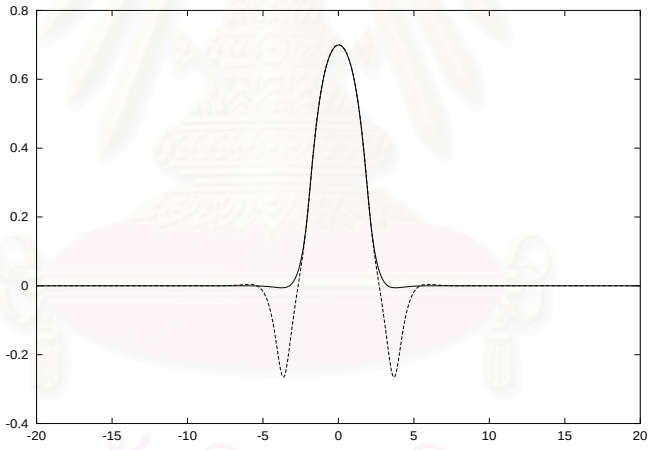

Figure 5.10: Typical free surface profiles for $\tau = 0.25$, $F = 0.7416$ and $\epsilon = -4.0$.

For larger negative forcing ($\epsilon = -4.0$), the turning point on the solution curve becomes very sharp. The portions of the solution curve before and after the turning point coincide despite the difference in the profiles. Figure 5.10 shows two elevation wave solutions at the same value of F. They have the same value of $y(0)$. These results suggest us that the displacement $y(0)$ is not a good quantity to measure in

this case. The appropriate quantity, probably, for larger ϵ is y_{max} which is defined as the distance between the crest and the trough of the elevation wave.

The development of wave profiles along the branch of $\epsilon = -0.01$ is depicted in Figures 5.11 - 5.13. Figures 5.11 and 5.12 refer to solutions along the lower portion of the curve before the turning point $F = F_4$, whereas Figure 5.13 corresponds to solution along the upper portion of the curve at the critical value $F = F_3$.

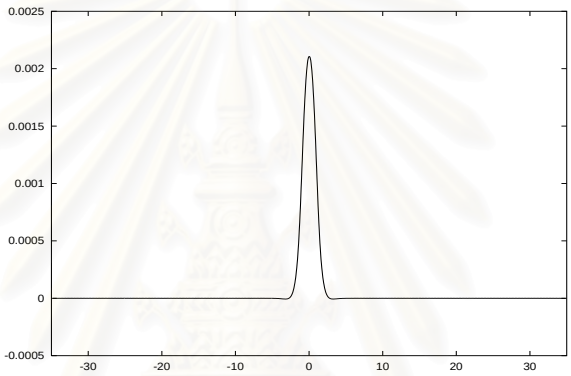

Figure 5.11: Typical free surface profile for $\tau = 0.25$, $F = 0.7416$ and $\epsilon = -0.01$.

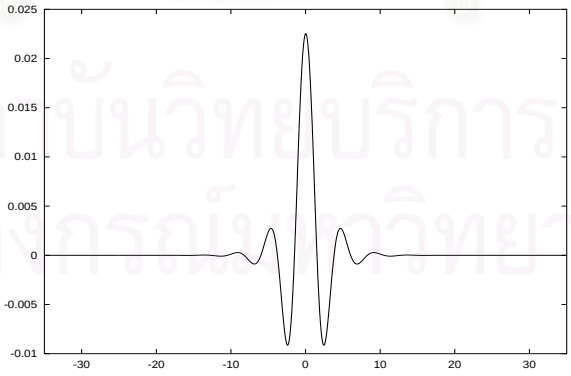

Figure 5.12: Typical free surface profile for $\tau = 0.25$, $F = 0.9618$ and $\epsilon = -0.01$.

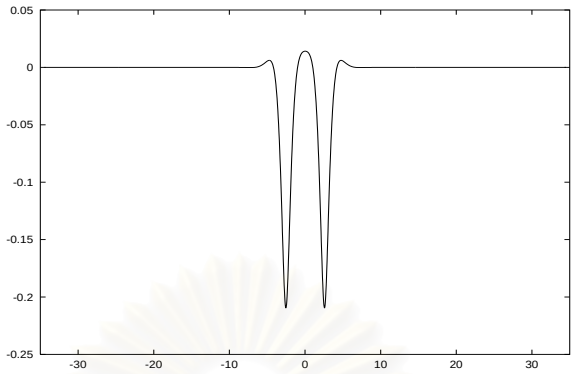

Figure 5.13: Typical free surface profile for $\tau = 0.25,\ F = 0.8602$ and $\epsilon = -0.01$.

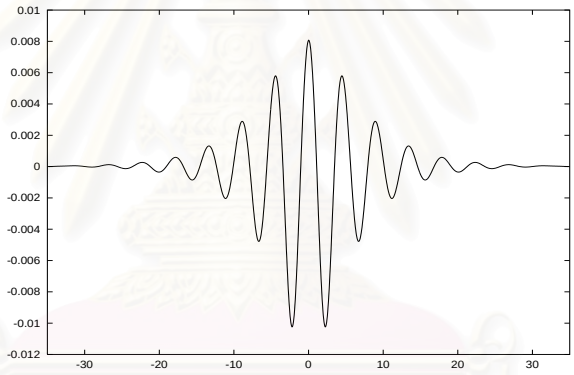

Figure 5.14: Typical free surface profile for $\tau = 0.25,\ F = 0.9695$ and $\epsilon = 0.0$.

The branch of an elevation solitary wave ($\epsilon = 0$) is also found and shown in Figure 5.9. It should be noted that these solutions bifurcate from the critical value F_m. A typical free surface profile of envelope solitary wave is shown in Figure 5.14. The connection to the weakly nonlinear theory of these solutions is discussed in Chapter 7.

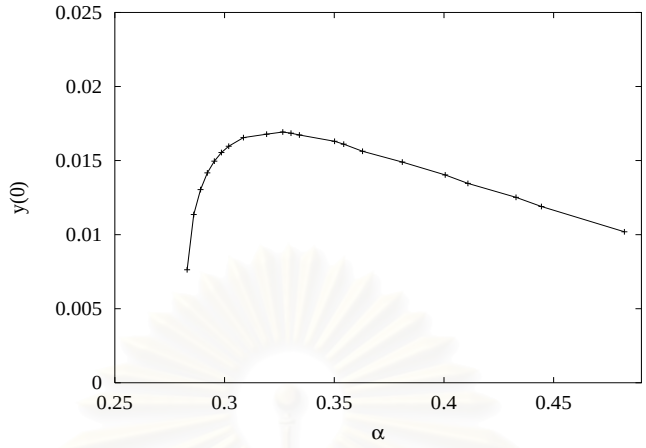

Figure 5.15: Relationship between α and $y(0)$ when $\epsilon = 0.0$, F is varied.

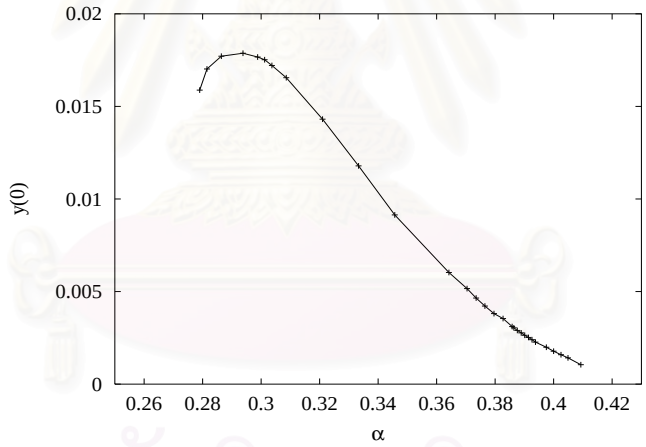

Figure 5.16: Relationship between α and $y(0)$ when $\epsilon = 0.0$, τ is varied.

Recently, a numerical study of gravity-capillary solitary waves in water of finite depth was reported by Dias, Menasce and Vanden-Broeck (1996). It is interesting to compare our results shown in Figure 5.9 to theirs. To do this, we define the dimensionless parameter

$$\alpha = \frac{\tau}{F^4}.$$

The branch of elevation solitary wave is replotted to show the relationship between α and $y(0)$. To vary α, we fix $\tau = 0.25$ and then vary for F $(0.866 < F < 0.975)$. As a consequence, α is varied between $0.444 > \alpha > 0.277$. The relationship between α and $y(0)$ for fixed τ is shown in Figure 5.15. Similarly, we can vary α by fixing $F = 0.9486$. This is equivalent to using τ in the range $(0.224, 0.333)$ which corresponds to $\alpha \in (0.276, 0.412)$. The relationship between α and $y(0)$ for a given value of F is shown in Figure 5.16.

The development of free surface profiles on the curve of Figure 5.16 is shown in Figures 5.17 - 5.19. As α decreases, more inflexion points in the wave profile become apparent. We are unable to find solutions for $\alpha < 0.276$. In addition, the wave amplitude approaches zero as α increases.

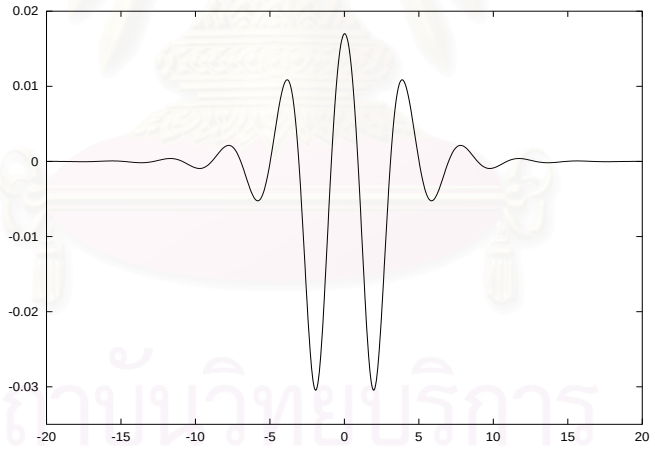

Figure 5.17: Typical free surface profile for $\tau = 0.228$, $F = 0.9486$ and $\alpha = 0.281$.

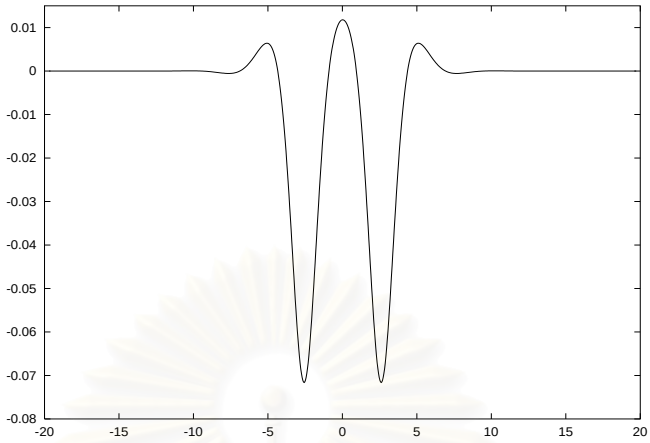

Figure 5.18: Typical free surface profile for $\tau = 0.270,\ F = 0.9486$ and $\alpha = 0.331$.

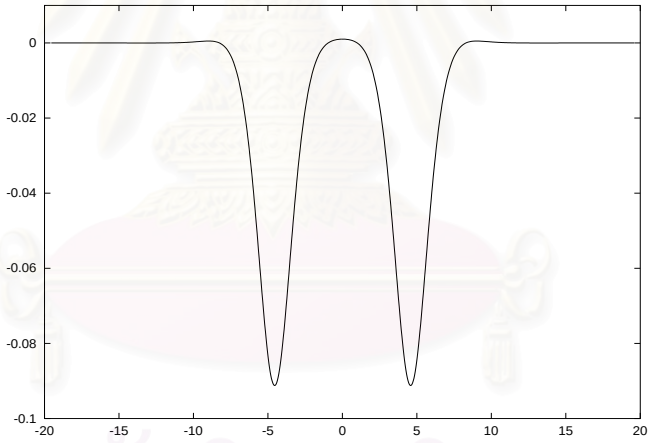

Figure 5.19: Typical free surface profile for $\tau = 0.333,\ F = 0.9486$ and $\alpha = 0.412$.

In our computations, the interesting quantities corresponding to the free surface profiles in Figures 5.17 - 5.19 are shown in Table 5.1.

Figure	τ	F	α	$y(0)$	$y''(0)$
5.17	0.228	0.948	0.281	0.017	-0.045
5.18	0.270	0.948	0.331	0.011	-0.023
5.19	0.333	0.948	0.412	0.001	-0.001

Table 5.1: Show flow parameter values correspond to Figures 5.17-5.19.

The relationship between $y(0)$ and $y''(0)$ presented in Table 5.1 is shown in Figure 5.20. It should be noted that Dias, Menasce and Vanden-Broeck defined $T/\rho U^2$ as a unit length. Therefore the scaling factor of the length scale as compared to ours differ by $F^2\alpha$. After adjusting this scaling factor we find that the curve in Figure 5.16 of our work is in good agreement with theirs. This constitutes an accuracy check of our numerical computations.

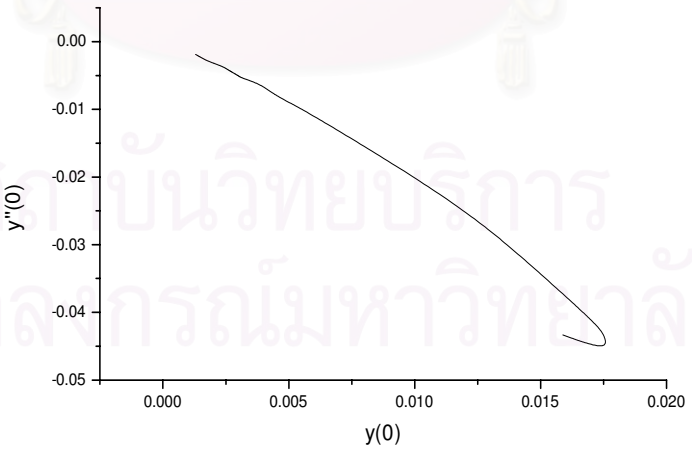

Figure 5.20: Relationship between $y(0)$ and $y''(0)$.

Moreover, we also found another kind of solution when $\tau = 0.25$ and $\epsilon = 0$. The wave profile is in the form of a two-humped solution (Figure 5.21).

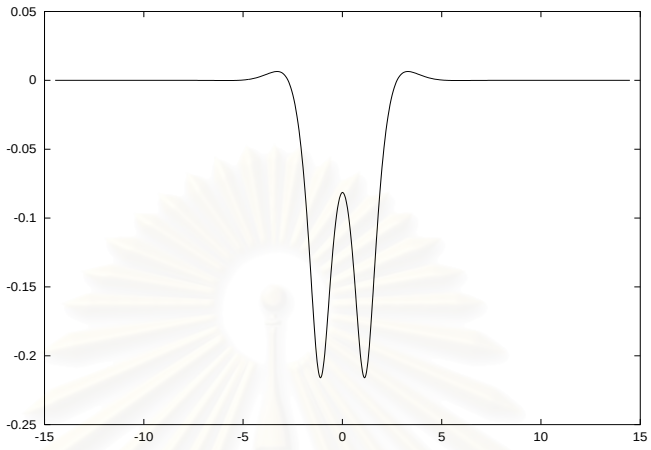

Figure 5.21: Typical free surface profile for $\tau = 0.25$, $F = 0.8602$ and $\epsilon = 0.0$.

The solution shown in Figure 5.21 is obtained by using the solution shown in Figure 5.13 as an initial guess. It requires 18 iterations for Newton's method to achieve the converged solution. We have also checked accuracy of this solution by increasing the number of mesh points. It is found that the solution is not sensitive to the number of mesh points. Moreover, to ensure that this solution actually exists, we use the two humps solution of $\epsilon = 0.0$ to be an initial guess of $\epsilon = -0.01$ solution (reverse direction). It is found that the converged solution is still in the form of two humps solution. Then, from our numerical investigation, we conclude that the two humps solution exists and the existence of this type of solution was also presented before by Dias, Menasce and Vanden-Broeck (1996).

As F increases, the wave profile (Figure 5.22) develops more inflexion points. When F decreases, the distance between the undisturbed level and the humps increases (Figure 5.23).

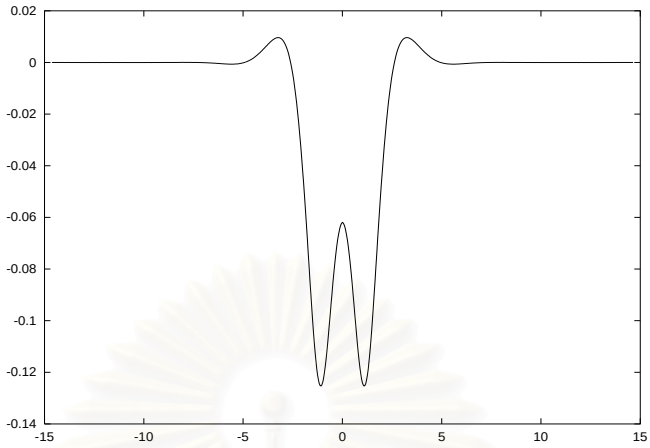

Figure 5.22: Typical free surface profile for $\tau = 0.25,\ F = 0.9165$ and $\epsilon = 0.0$.

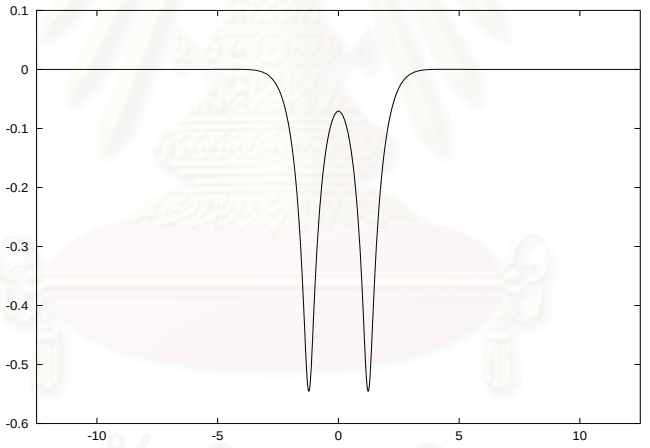

Figure 5.23: Typical free surface profile for $\tau = 0.25,\ F = 0.6323$ and $\epsilon = 0.0$.

Next, to understand the effects of a pressure distribution on these two-hump solutions, we vary $\epsilon > 0$ and < 0. The wave profiles for increasing $\epsilon > 0$ are shown in Figures 5.24 - 5.26.

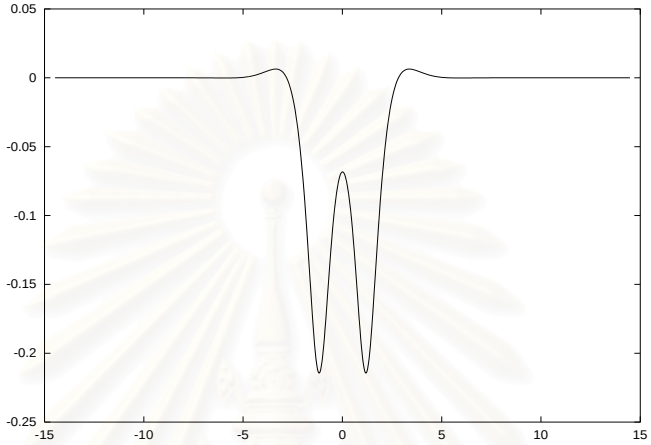

Figure 5.24: Typical free surface profile for $\tau = 0.25$, $F = 0.8602$ and $\epsilon = 0.01$.

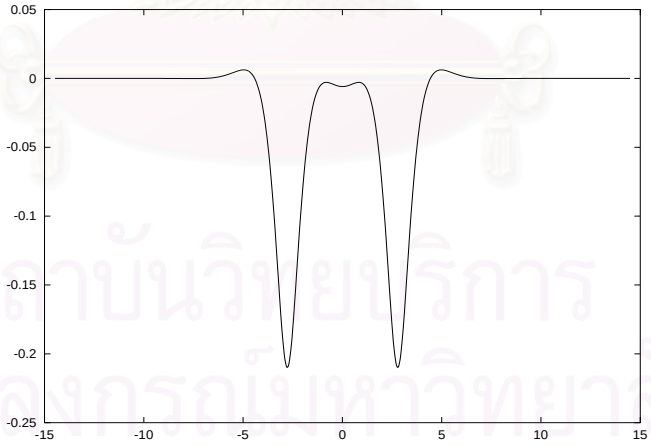

Figure 5.25: Typical free surface profile for $\tau = 0.25$, $F = 0.8602$ and $\epsilon = 0.03$.

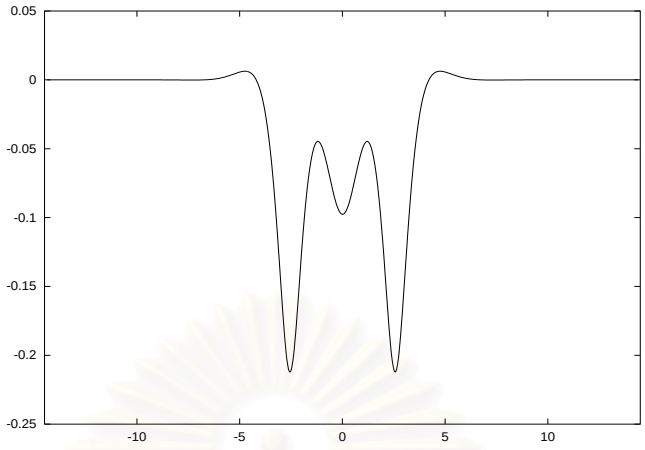

Figure 5.26: Typical free surface profile for $\tau = 0.25$, $F = 0.8602$ and $\epsilon = 0.15$.

In our calculations, we perturb the solution shown in Figure 5.21 with small value of $\epsilon > 0$. The increment of ϵ value is 0.01. In doing so we can obtain the solutions when $\epsilon = 0.01, 0.02, ...$ when F and τ are fixed. We found that the wave profile when $\epsilon = 0.02$ is similar to the profile shown in Figure 5.24. Surprisingly, the free surface profile when $\epsilon = 0.03$ is different from the case of $\epsilon = 0.02$ and the calculation requires 20 iterations for Newton's method to reach the converged solution. It shows that the behavior at the origin changes rapidly as ϵ varies. These results suggest us to probe the behavior of solutions in the neighborhood of $\epsilon = 0.02$. To do this, we use the increment of value of ϵ with 0.001. We obtain the converged solution when $\epsilon = 0.021, 0.022, 0.023$ and 0.024. These wave profiles appear to have similar pattern to the one in Figure 5.24. No solutions can be obtained when $\epsilon = 0.025$. We conjecture that the value of ϵ approaches a critical value that a new family of solution can be found (Figure 5.25). From the solution when $\epsilon = 0.03$, we futher increase the value of ϵ until $\epsilon = 0.15$ (Figure 5.26). The wave profile develops more humps as ϵ increases. To ensure the accuracy of solution, we increase the number of mesh points and decrease the mesh spacing until the wave profile is unchanged within graphical

accuracy.

It should be noted that these multi-hump solutions apparently exist only for a small range of Froude number, and that $y(0) < 0$. Due to the complexity in their solution structure, we do not show this solution branch in Figure 5.9.

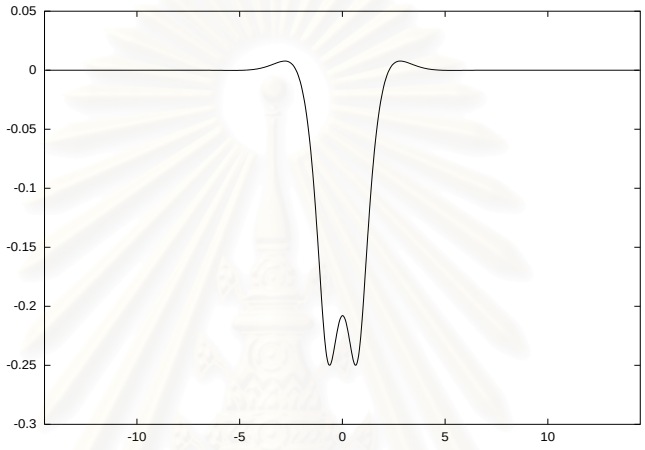

Figure 5.27: Typical free surface profile for $\tau = 0.25$, $F = 0.8602$ and $\epsilon = -0.3$.

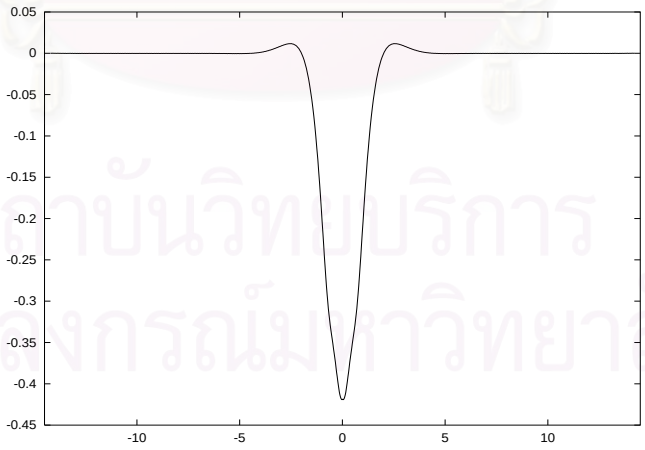

Figure 5.28: Typical free surface profile for $\tau = 0.25$, $F = 0.8602$ and $\epsilon = -2.5$.

We observe from Figures 5.27 and 5.28 that in order to get relatively similar wave amplitudes $y(0)$ for the case when $\epsilon < 0$ it is necessary to increase considerably the magnitude of ϵ. This shows the dominant role of surface tension in the dynamic boundary condition.

Next, we will investigate whether or not there exist a branch of solutions for positive forcing $\epsilon > 0$. Here we choose a solution from the unforced branch $\epsilon = 0$ in Figure 5.9 and then to vary ϵ by increasing its value. The converged solution (Figure 5.29) that we choose is at $F = 0.9110$. We perturb this solution by a small value of $\epsilon = 0.001$. The result is similar to the wave profile shown in Figure 5.29. Again, we perturb the solution $\epsilon = 0.001$ by $\epsilon = 0.005$. We obtain a new solution (Figure 5.30) that there is a dimple at the origin. The solutions for larger $\epsilon > 0$ are also calculated and shown in Figures 5.31 and 5.32.

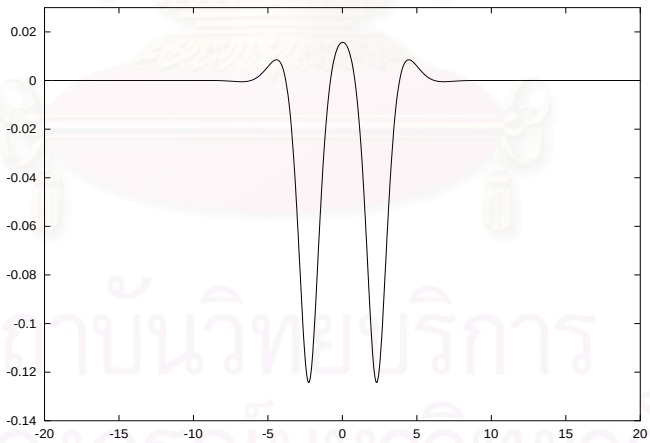

Figure 5.29: Typical free surface profile for $\tau = 0.25$, $F = 0.9110$ and $\epsilon = 0.0$.

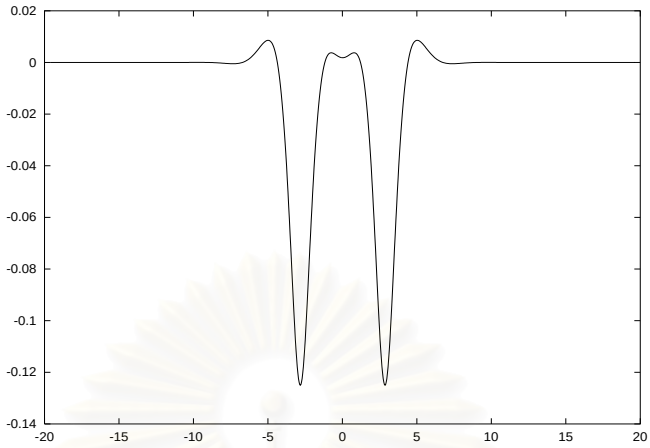

Figure 5.30: Typical free surface profile for $\tau = 0.25$, $F = 0.9110$ and $\epsilon = 0.01$.

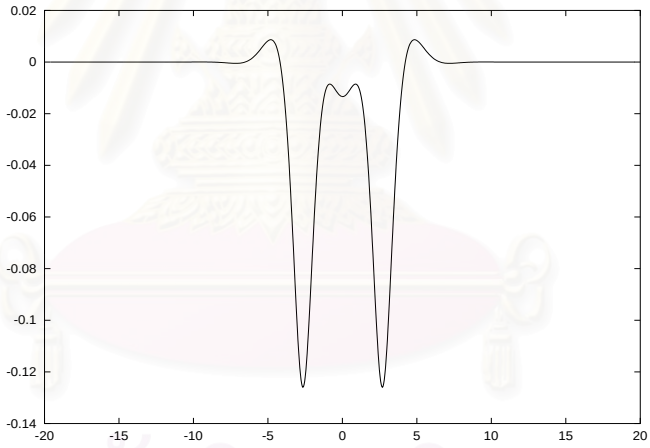

Figure 5.31: Typical free surface profile for $\tau = 0.25$, $F = 0.9110$ and $\epsilon = 0.03$.

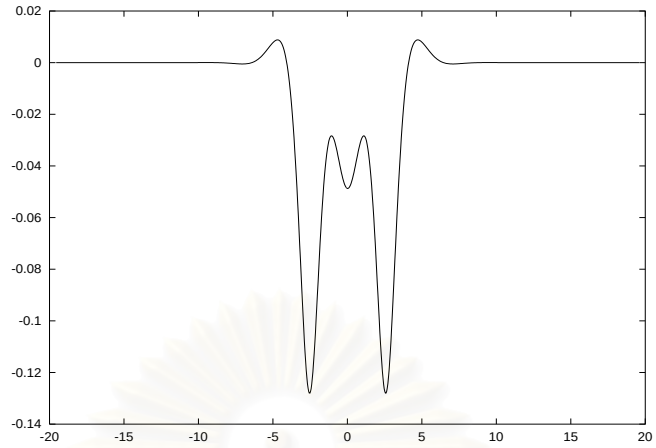

Figure 5.32: Typical free surface profile for $\tau = 0.25$, $F = 0.9110$ and $\epsilon = 0.055$.

We can see that the value of $y(0)$ changes sign from positive to negative as ϵ increases. In this case, the value of $y(0)$ is not a good quantity to describe such waves. From this observation, we conclude that, for $\epsilon > 0$ and very small, the elevation waves do exist.

Note that the wave profiles shown in Figure 5.31 and Figure 5.25 are in the same family because, as F decreases from 0.911 to 0.8602, the wave profile in Figure 5.31 is identical to the profile in Figure 5.25.

Finally, let us investigate the effects of Froude number on the wave profile in Figure 5.30. That is we fix the value of τ and ϵ and then vary F. As F decreases, the free surface profile for $F = 0.8631$ is shown in Figure 5.33. Comparing this profile with the one in Figure 5.24, we find that these solutions are not identical (differ by 2 decimal places of F). This shows the non-uniqueness of forced elevation wave solutions. As F increases, the free surface profile for $F = 0.9539$ is shown in Figure 5.34. The wave profile develops more inflexion points as $F \to 1$. We are unable to obtain solutions when $F > 0.9539$ because more mesh points are needed to capture small waves on the free surface.

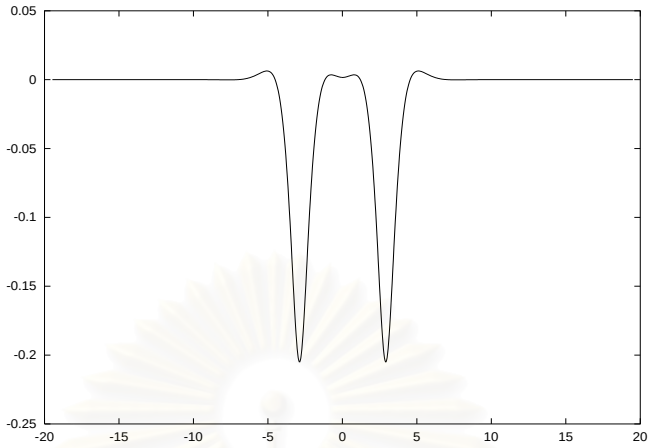

Figure 5.33: Typical free surface profile for $\tau = 0.25,\ F = 0.8631$ and $\epsilon = 0.01$.

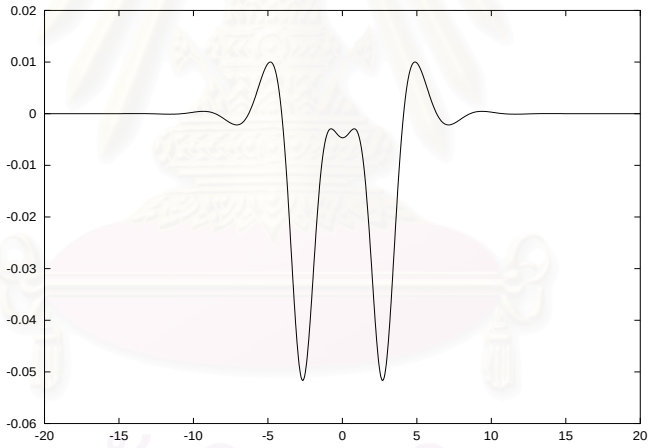

Figure 5.34: Typical free surface profile for $\tau = 0.25,\ F = 0.9539$ and $\epsilon = 0.01$.

CHAPTER VI

WEAKLY NONLINEAR THEORY

Forced Korteweg-de Vries Equation

The theory of linearized wave described in Chapter 2 is valid when the waves have relatively small amplitude. Some nonlinear effects need to be taken into account in the dynamic boundary condition to give more accurate model. One of the powerful method to add some nonlinear effects is the perturbation method. This then leads us to the development of weakly nonlinear theory. As F approaches 1, certain fully nonlinear solutions described in Chapter 4 ($\tau > 1/3$) are monotonic type with very large wavelength such that this form of wave solution is the well known "solitary" wave. One of the famous weakly nonlinear model to describe such solitary wave solutions is known as the Korteweg and de Vries (KdV) equation.

Generally, the KdV equation predicts the solitary wave without forcing term. To make the connection between the fully nonlinear results described earlier in Chapter 4 and the KdV model, we need to add the localized pressure term into the dynamic boundary condition. Then the KdV equation with specific forcing term will be derived (Section 6.1) and refered to as the forced KdV equation (fKdV). Some aspects from the fKdV equation with various forms of forcing are discussed in Section 6.2. Finally, the comparisons between the nonlinear results and the fKdV solutions are also presented in Section 6.3.

6.1 Derivation of the forced KdV Equation

Consider a uniform stream of velocity U in a fluid domain of finite depth H and Cartesian coordinates with the x-axis along the undisturbed free-surface level and the y-axis vertically upwards. Fluid is assumed to be inviscid and incompressible and the flow is irrotational. Gravity is acting in the negative y-direction. Surface tension is also included in our problem. We choose U, H and UH as velocity, length and velocity potential scales respectively. Subject to these normalization, the governing equations in terms of potential function $\phi(x, y)$ can be derived.

$$\phi_{xx} + \phi_{yy} = 0, \quad -\infty < x < \infty, -1 < y < \eta(x) \tag{6.1}$$

$$\phi_y = 0, \quad y = -1 \tag{6.2}$$

$$\phi_y = \phi_x \eta_x, \quad y = \eta(x) \tag{6.3}$$

$$\frac{F^2}{2}(\phi_x^2 + \phi_y^2 - 1) + \eta = \tau \frac{\eta_{xx}}{(1+\eta_x^2)^{3/2}} - \frac{F^2}{2}\,\epsilon p(x), \quad y = \eta(x) \tag{6.4}$$

Here F is the Froude number $U/\sqrt{gH}$, τ is the Bond number $T/\rho g H^2$ and $\epsilon p(x)$ is the pressure forcing term $p_a(x)/\rho U^2$. Perturbation method is used to extract certain nonlinear effects in the fully nonlinear water wave equations. We assume that the wave is small amplitude when comparing with the fluid depth. Thus we put $\xi = \mu x$ for $\mu \ll 1$ and expand η and ϕ as

$$\eta = \mu^2 A(\xi) + \mu^4 \eta_2(\xi) + ...$$

$$\phi = x + \phi_1(\xi, y) + \mu\phi_2(\xi, y) + ...$$

Substituting these expansions into equations (6.1) and (6.2), thus

$$[\ \phi_{1yy} + \mu\phi_{2yy} + ...\ ]\ +\ \mu^2\,[\ \phi_{1\xi\xi} + \mu\phi_{2\xi\xi} + ...\ ]\ =\ 0,\ \ -1 < y < \eta(x)$$

and

$$\phi_{1y} + \mu\phi_{2y} + \mu^2\phi_{3y}\ =\ 0,\ \ y = -1\,.$$

Equating coefficients of the same power of μ,

μ^0:
$$\phi_{1yy}\ =\ 0,\ \ -1 < y < 0,$$
$$\phi_{1y}\ =\ 0,\quad y = -1.$$

This implies that ϕ_1 is function of ξ only, say $\phi_1 = B_1(\xi)$.

μ^1:
$$\phi_{2yy}\ =\ 0,\ \ -1 < y < 0,$$
$$\phi_{2y}\ =\ 0,\quad y = -1.$$

Again, ϕ_2 is function of ξ only, say $\phi_2 = B_2(\xi)$.

μ^2:
$$\phi_{3yy} + \phi_{1\xi\xi}\ =\ 0,\ \ -1 < y < 0,$$
$$\phi_{3y}\ =\ 0,\qquad y = -1.$$

Thus, $\phi_3\ =\ -\frac{1}{2}B_{1\xi\xi}(y+1)^2\ +\ B_3(\xi)$.

μ^3:
$$\phi_{4yy} + \phi_{2\xi\xi}\ =\ 0,\ \ -1 < y < 0,$$
$$\phi_{4y}\ =\ 0,\qquad y = -1.$$

Similarly, $\phi_4\ =\ -\frac{1}{2}B_{2\xi\xi}(y+1)^2\ +\ B_4(\xi)$.

μ^4:
$$\phi_{5yy} + \phi_{3\xi\xi}\ =\ 0,\ \ -1 < y < 0,$$
$$\phi_{5y}\ =\ 0,\qquad y = -1.$$

Thus, $\phi_5\ =\ \frac{1}{24}B_{1\xi\xi\xi\xi}(y+1)^4\ -\ \frac{1}{2}B_{3\xi\xi}(y+1)^2\ +\ B_5(\xi)$.

We can see that the above inspection leads us to consider a new expansion in the odd power of small parameter μ,

$$\phi = x + \mu\phi_1 + \mu^3\phi_2 + \mu^5\phi_3 + ...$$

where

$$\phi_1 = B(\xi),$$

$$\phi_2 = -\tfrac{1}{2}B_{\xi\xi}(y+1)^2 + B_1(\xi),$$

$$\phi_3 = \tfrac{1}{24}B_{\xi\xi\xi\xi}(y+1)^4 - \tfrac{1}{2}B_{1\xi\xi}(y+1)^2 \ .$$

From the free surface boundary conditions, we expand ϕ_x and ϕ_y around the undisturbed free surface level $(y = 0)$

$$\phi_y\,|_{y=\eta} \ = \ \phi_y\,|_{y=0} + \eta\phi_{yy}\,|_{y=0} + \frac{\eta^2}{2}\phi_{yyy}\,|_{y=0} + ...,$$
$$\phi_x\,|_{y=\eta} \ = \ \phi_x\,|_{y=0} + \eta\phi_{xy}\,|_{y=0} + \frac{\eta^2}{2}\phi_{xyy}\,|_{y=0} + ...$$

So, from the kinematic boundary condition, we have

$$\phi_y + \eta\phi_{yy} + ... \ = \ (\phi_x + \eta\phi_{xy} + ...)\eta_x$$

or,

$$[\,\mu\phi_{1y} + \mu^3\phi_{2y} + \mu^5\phi_{3y} + ...\,] + [\,\mu^2 A + \mu^4\eta_2 + ...\,][\,\mu\phi_{1yy} + \mu^3\phi_{2yy} + ...\,]$$
$$= \ [\,1+\mu^2\phi_{1\xi}+\mu^4\phi_{2\xi}+...+(\mu^2 A+\mu^4\eta_2+...)(\mu\phi_{1xy}+\mu^3\phi_{2xy}+...)+...\,][\,\mu^3 A_\xi+\mu^5\eta_{2\xi}+...].$$

Next, we equate coefficients of the same power of μ.

μ^1: $$\phi_{1y} \ = \ 0, \ \ y = 0$$

which is automatically satisfied.

μ^3: $$\phi_{2y} + A\phi_{1yy} \;=\; A_\xi\,,\;\; y = 0$$

or, $$-B_{\xi\xi}(y+1) \;=\; A_\xi\,.$$

Integrating the above equation with respect to ξ, we get $B_\xi = -A(\xi) \,+\, \text{const}.$

μ^5: $$\phi_{3y} + A\phi_{2yy} + \eta_2\phi_{1yy} \;=\; \eta_{2\xi} \,+\, A_\xi\phi_{1\xi}\,,\;\; y = 0\,,$$

or, $$\tfrac{1}{6}B_{\xi\xi\xi\xi}(y+1)^3 - B_{1\xi\xi}(y+1) - AB_{\xi\xi}(y+1) \;=\; \eta_{2\xi} + A_\xi B_\xi\,.$$

Thus, $B_{1\xi\xi} = -\frac{1}{6}A_{\xi\xi\xi} + 2AA_\xi - \eta_{2\xi}$. Integrating with respect to ξ from 0 to ξ, we obtain $B_{1\xi} = -\frac{1}{6}A_{\xi\xi} + A^2 - \eta_2 + \text{const}.$

Next, we expand the Froude number as

$$F^2 \;=\; 1 \,+\, \mu^2\Delta \,+ ....$$

Substituting this into the Bernoulli equation, we have

$$\frac{1}{2}(1+\mu^2\Delta + ...)\,\{\,(1 + \mu^2 B_\xi - \mu^4\frac{B_{\xi\xi\xi}}{2} + \mu^4 B_{1\xi} + ...)^2 \,+\, (-\mu^3 B_{\xi\xi} + ...)^2 - 1\}$$

$$+\,(\mu^2 A + \mu^4\eta_2 + ...) \;=\; \tau\mu^4 A_{\xi\xi} + ... - \frac{1}{2}\,\epsilon p(x)\,.$$

Then,

$$(1+\mu^2\Delta + ...)\{\mu^2 B_\xi - \mu^4\frac{B_{\xi\xi\xi}}{2} + \mu^4 B_{1\xi} + \mu^4\frac{B_\xi^2}{2} + ...\}$$

$$+\,(\mu^2 A + \mu^4\eta_2 + ...) \;=\; \tau\mu^4 A_{\xi\xi} + ... - \frac{1}{2}\,\epsilon p(x)\,.$$

After substituting $B_{1\xi}$ and collecting the coefficients of μ^4, we obtain

$$-\Delta A \,+\, \frac{3}{2}A^2 \,+\, (\frac{1}{3} - \tau)A'' \,+\, \frac{\epsilon}{2\mu^4}p(x) \;=\; 0\,. \tag{6.5}$$

The primes in equation (6.5) denote derivatives with respect to ξ. Here $p = p(\xi/\mu)$. Equation (6.5) is the steady fKdV equation. It has been extensively discussed in the

literature (see for instance, Dias and Vanden-Broeck (2002) for a recent comprehensive account in the present context).

The fKdV equation balances between small nonlinear term and dispersive term and also includes the effect of pressure distribution as a source term. From the expansions of F and η, we can see that the fKdV equation provides us good predictions when the flow parameter F closes to 1 and wave is small amplitude. The dispesive term disappears when the value of τ approaches $1/3$. It is a critical value of our problem as discussed earlier in the linear theory analysis. This shows the overlaped agreement between weakly nonlinear and linear theories. In general, now we can extend the analysis from the linear theory to the wave solution in case of very large wavelength. Next, we will analyze the solutions of the fKdV equation to predict the bifurcation of depression and elevation waves. Such details will be disscussed in the next section.

6.2 Solutions of the forced KdV Equation

In order to facilitate comparison with the numerical solutions of the fully nonlinear problem, we rewrite equation (6.5) in the unscaled coordinates

$$(F^2-1)\eta - \frac{3}{2}\eta^2 + (\tau - \frac{1}{3})\eta_{xx} = \frac{1}{2}\epsilon p(x)\,. \tag{6.6}$$

However, before discussing the numerical solution of (6.6) with the same forcing function $p(x)$ as that used in the fully nonlinear numerical solutions, reduced appropriately for the present long-wave limit (see (6.17) below), it is useful to discuss some explicit solutions of the fKdV equation (6.6) for various simplified forcing functions.

First, we approximate $p(x)$ with a δ-function so that (6.6) becomes

$$(F^2-1)\eta - \frac{3}{2}\eta^2 + (\tau - \frac{1}{3})\eta_{xx} = \frac{\epsilon p_0}{2}\delta(x), \tag{6.7}$$

$$\text{where} \qquad p_0 = \int_{-\infty}^{\infty} p(x)\,dx\,.$$

This situation arises if, in the derivation of the fKdV equation (6.5), one supposes that, the pressure forcing term scales with the original variable x rather than the scaled variable ξ. In this case the pressure forcing term in (6.5) is $p(x) = p(\xi/\mu)$, and the limit $\mu \to 0$ then yields the δ-function (Akylas (1993)).

The fKdV equation (6.7) with this δ-function forcing has been comprehensively discussed by Dias and Vanden-Broeck (2002) using phase-plane methods. Here we proceed a little differently and seek symmetric localized solutions directly, as follows,

$$\text{either} \qquad \eta(x) = a\ \text{sech}^2\gamma(x-x_0) \quad \text{for} \quad x>0 \tag{6.8a}$$

$$\text{or} \qquad \eta(x) = \frac{a}{\sinh^2\gamma(x-x_0)} \quad \text{for} \quad x>0 \tag{6.8b}$$

$$\text{where, either} \qquad F^2-1 = a \quad \text{and} \quad a = -4(\tau - \frac{1}{3})\gamma^2 \tag{6.9a}$$

$$\text{or} \qquad F^2 - 1 = -a \quad \text{and} \quad a = 4(\tau - \frac{1}{3})\gamma^2. \tag{6.9b}$$

The corresponding solutions in $x < 0$ are obtained by imposing symmetry ($\eta(x) = \eta(-x)$). Here for case (a) (that is, (6.8a, 6.9a)), $a < 0$ since $\tau > 1/3$ and so this solution can only describe depression waves, while for case (b) (that is, (6.8b, 6.9b)), $a > 0$ and so this solution describes elevation waves. Note that in case (a) we can allow $x_0 >$ or < 0, but that in case (b) only the case $x_0 < 0$ is allowed to avoid singular solutions.

Next we must use the jump condition at $x = 0$, obtained by integrating (6.7) across a small interval about the origin,

$$(\tau - \frac{1}{3})\ [\eta_x]_{0-}^{0+} = \frac{\epsilon p_0}{2}\,.$$

Hence we get

$$\text{either} \qquad 4a\gamma\ \text{sech}^2(\gamma x_0)\tanh(\gamma x_0) = \frac{\epsilon p_0}{2(\tau - \frac{1}{3})} \tag{6.10a}$$

$$\text{or} \qquad 4a\gamma \frac{\coth(\gamma x_0)}{\sinh^2(\gamma x_0)} = \frac{\epsilon p_0}{2(\tau - \frac{1}{3})}\,. \tag{6.10b}$$

These respectively determine x_0 in terms of ϵ and a and so complete the solution. For a given F we can determine a, γ from (6.9a,b) and finally x_0 from (6.10a,b) respectively. Note that the central amplitude is $\eta(0) = a\ \text{sech}^2(\gamma x_0)$ in case (a) and $\eta(0) = a/\sinh^2(\gamma x_0)$ in case (b). We now see that in case (a) there are two branches of depression waves ($\eta(0) < 0$); one exists for $\epsilon > 0$ and is monotonic in $x > 0$ since $x_0 < 0$; the other exists for $\epsilon < 0$ and is dimpled at the origin since $x_0 > 0$, that is, the minimum of $\eta(x)$ occures at $x_0 > 0$ and not at the origin, which is a local maximum instead. The bifurcation curve, that is the graph of $\eta(0)$ versus F is the same for both branches, and is given by

$$(\epsilon p_0)^2 = 16\,\eta^2(0)(\tau - \frac{1}{3})(\eta(0) - [F^2 - 1])\,. \tag{6.11}$$

The monotonic solution branch is as expected, and agrees qualitatively with the numerical solutions. However, the dimpled solution branch lies above the unforced solitary wave curve ($\epsilon = 0$ so that $\eta(0) = F^2 - 1$ in this present fKdV approximation), whereas it is expected to lie below the unforced branch (see Figures 6.2 and 6.3 below). This discrepancy is partly explained in the fully nonlinear numerical results that a dimpled solution does arise, but only when F is sufficiently close to 1 and then the branch does indeed cross the unforced branch (see Figure 4.1). Next, for case (b) there is only one branch, an elevation wave with $\epsilon < 0$, in qualitative agreement with the numerical solutions (see Figure 4.8). The bifurcation curve is again given by (6.11).

The δ-function forcing approximation omits the forcing length scale x_b and this may explain why it yields only qualitative agreement with the numerical solutions. Hence we now replace the δ-function with a smooth forcing term, $a\,\mathrm{sech}^2(\gamma x)$, so that in (6.6)

$$p(x) = \frac{p_0}{2\gamma}\,\mathrm{sech}^2(\gamma x)\,. \tag{6.12}$$

Here, the area under the forcing function is p_0 and there is an imposed length scale of γ^{-1}. In this case we seek an explicit solution

$$\eta = a\,\mathrm{sech}^2(\gamma x)\,. \tag{6.13}$$

We find that

$$a = -4\gamma^2(\tau - \frac{1}{3}) \quad \text{and} \quad (F^2 - 1)a - a^2 = \frac{\epsilon p_0}{2\gamma}\,. \tag{6.14}$$

Elimination of γ yields the bifurcation branches. Note that here $a = \eta(0) < 0$ and $\epsilon > 0 (< 0)$ gives $F^2 - 1 < (>) a$. Thus the branch lying below the unforced branch is now found, but does not develop a dimple. Also, there is no elevation wave branch for this particular solution, although presumably this can be found by numerical integration of (6.12). Further it is anomalous in that the branch with $F^2 - 1 > a$

extends to the forbidden region $F > 1$. The reason is that here the forcing (6.12) extends to infinity, unlike the δ-function forcing in (6.7) and the solution (6.13) has the same decay rate at infinity as the forcing. Hence the usual argument about why $F > 1$ does not apply.

This suggests that (6.12) is not a good choice as forcing term and a better one is

$$p(x) = \frac{3p_0}{4\gamma}\mathrm{sech}^4(\gamma x)\,. \tag{6.15}$$

Here, the area under the forcing function is again p_0. In this case we again seek an explicit solution of the form (6.13) (which now decays more slowly at infinity than the forcing term) and we find that

$$F^2 - 1 = -4\gamma^2(\tau - \frac{1}{3}) \quad \text{and} \quad (F^2-1)a - a^2 = \frac{\epsilon p_0}{2\gamma}\,. \tag{6.16}$$

Note that the bifurcation curve in (6.16) is in fact identical to (6.14) but now $F < 1$ as required. Also, the expression (6.16) includes the branch with $\eta(0) = a > 0$ which (6.14) does not allow. Hence we conclude that the forcing term (6.15) is preferable to both the δ-function forcing term and to (6.12).

We now return to the fKdV equation (6.6) and choose the forcing term to be the same as that used in the fully nonlinear calculations, but reduced here to the appropriate form for the weakly nonlinear and weakly dispersive limit, that is

$$p(x) = F^2 \exp[\frac{{x_b}^2}{x^2 - {x_b}^2}] \quad \text{for} \quad |x| < |x_b|\,, \tag{6.17}$$

and is zero elsewhere. Note that although a strict adherence to the asymptotic limit would require us to put $F^2 = 1$ in (6.17), we will keep it to ensure an improved agreement with the numerical solutions as F departs from 1. To solve (6.6) numerically, we set "initial" conditions at $x = L$

$$\eta(L) = a_0 \exp(-2\gamma L)\,, \quad \eta_x(L) = -2\gamma a_0 \exp(-2\gamma L)\,, \tag{6.18}$$

$$\text{where} \quad (F^2 - 1) = -4(\tau - \frac{1}{3})\gamma^2 \,. \tag{6.19}$$

Here we choose $L >> x_b$ and sufficiently large so that η effectively satisfies the linearization of (6.6). Then we integrate (6.6) numerically by using a high-order Runge-Kutta routine from L to 0, adjusting a_0 until we can satisfy the symmetry condition $\eta_x(0) = 0$.

An alternative specification of the initial conditions is to solve (6.6) exactly in $x > x_b$. However, the numerical solutions obtained in this way are essentially identical to those using (6.18) and hence we shall give no details of this alternative procedure here.

6.3 Comparison of the fKdV equation with numerical solutions

6.3.1 Depression wave

We will compare the solutions of the fKdV equation (6.6) with the numerical solutions of the fully nonlinear equations, and also with the linear solution obtained from equation (2.9). Here we consider $\epsilon > 0$, $= 0$ and < 0. For a positive value of ϵ the branches of the linear, fKdV and nonlinear solutions when $\epsilon = 0.001$ are shown in Figure 6.1. This shows that the results from the fKdV model agree well with the fully nonlinear numerical results along the whole branch, while, as expected, agreement with the linear solution holds only for the bifurcation from the uniform flow branch (the upper curve) and only when F is not too close to 1. The corresponding free surface profiles for $\epsilon = 0.001$ are shown in Figure 6.4.

For unforced solutions ($\epsilon = 0$), the branches of fKdV and nonlinear solutions are shown in Figure 6.2 and there is again good agreement when F is close to 1.

For a negative value of ϵ the branches of fKdV and nonlinear solutions are shown in Figure 6.3. As F approaches 1 we find that the free surface profile develops a dimple (see Figure 6.5) and at the same time the bifurcation curve crosses the $\epsilon = 0$ branch. The agreement between the numerical results and the fKdV model persists up to $\epsilon = \pm 0.01$, but begins to fail as ϵ is increased further.

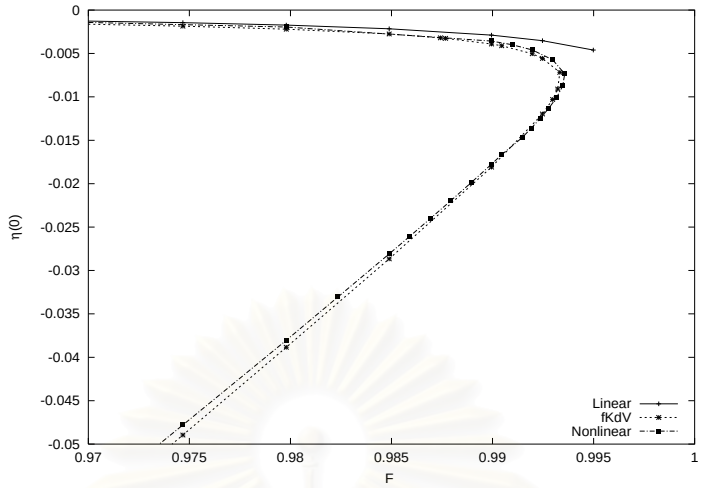

Figure 6.1: Relationship between F and $\eta(0)$ when $\tau = 0.4$, $\epsilon = 0.001$

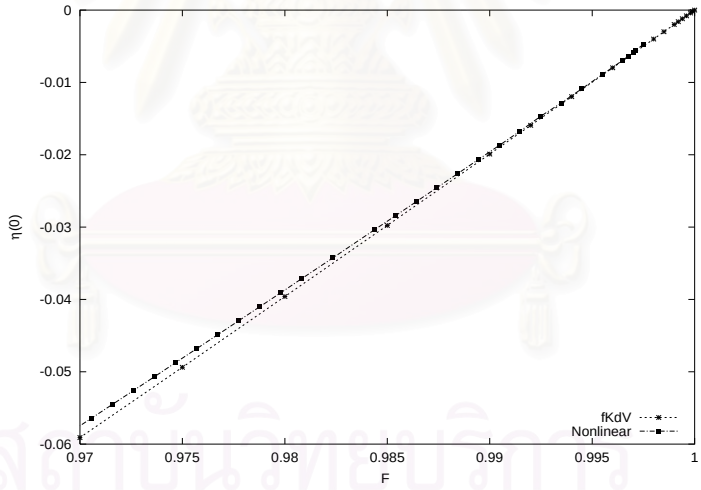

Figure 6.2: Relationship between F and $\eta(0)$ when $\tau = 0.4$, $\epsilon = 0$

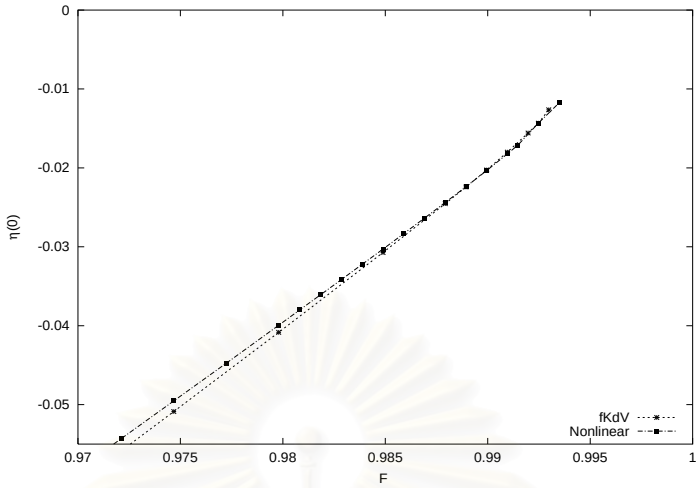

Figure 6.3: Relationship between F and $\eta(0)$ when $\tau = 0.4$, $\epsilon = -0.001$

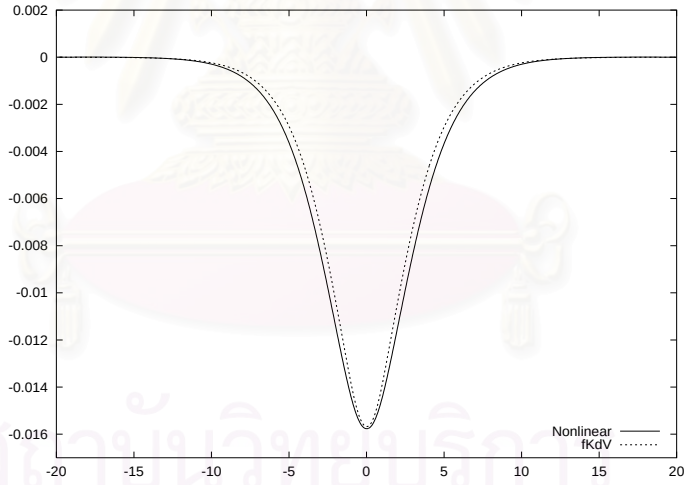

Figure 6.4: Typical free surface profiles when $\tau = 0.4$, $\epsilon = 0.001$ and $F = 0.9910$

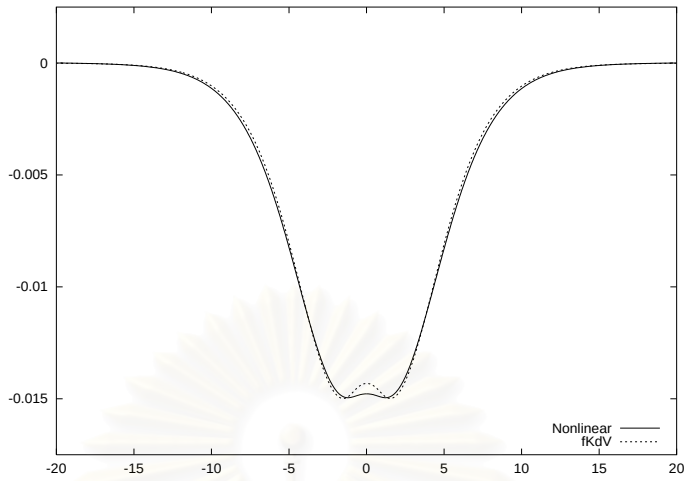

Figure 6.5: "Dimpled" free surface profiles when $\tau = 0.4$, $\epsilon = -0.001$ and $F = 0.9925$

6.3.2 Elevation wave

The elevation wave branch for $\tau > 1/3$ is a bifurcation from a uniform flow, and exist only for negative values of ϵ. Both the linear and fKdV solutions can predict this type of solution. For a small values of $\epsilon = -0.001$, the elevation wave can be viewed as a linear wave (Figure 6.6). In the case of negative pressure forcing $\epsilon = -0.1$, the role of nonlinear terms becomes more pronounced as F nears 1, and the linear theory fails to give a correct prediction (see Figure 6.7). But in this regime the fKdV model agrees well with the nonlinear results. The corresponding free surface profiles for $\epsilon = -0.1$ is shown in Figure 6.8.

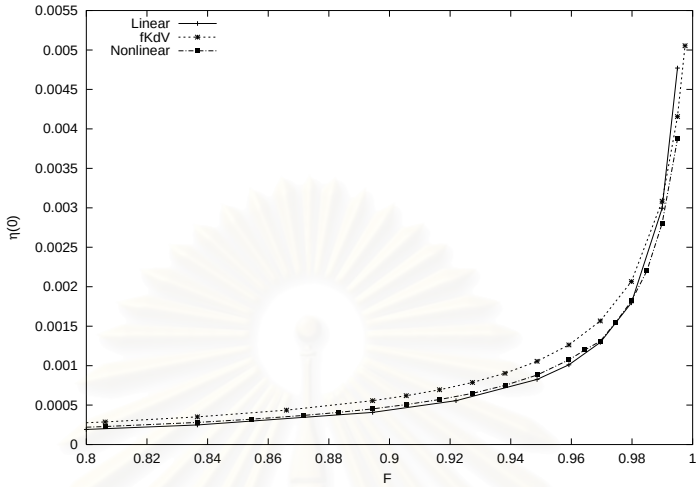

Figure 6.6: Relationship between F and $\eta(0)$ when $\tau = 0.4$, $\epsilon = -0.001$

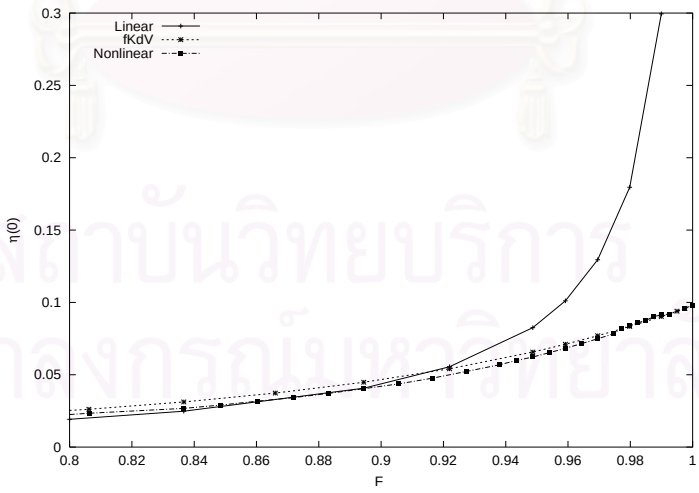

Figure 6.7: Relationship between F and $\eta(0)$ when $\tau = 0.4$, $\epsilon = -0.1$

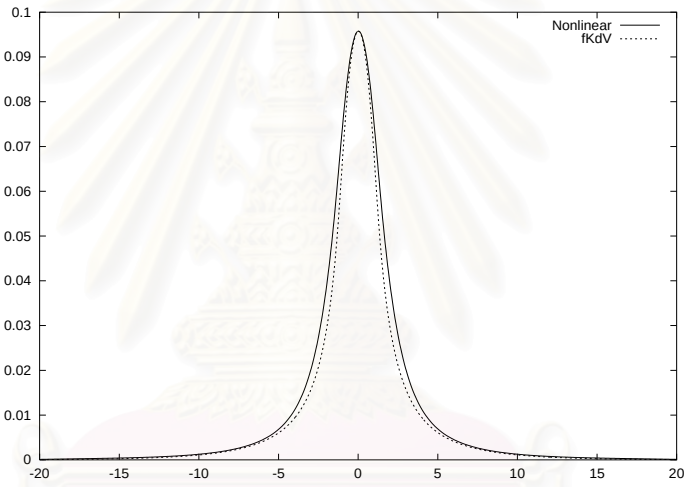

Figure 6.8: Typical free surface profiles when $\tau = 0.4$, $\epsilon = -0.1$ and $F = 0.9975$

CHAPTER VII

WEAKLY NONLINEAR THEORY

Forced Nonlinear Schrödinger Equation

In this Chapter, we confine our attention to the gravity-dominated case when $\tau < 1/3$ for both depression and elevation waves. The linearized theory in Chapter 2 reveals that in order to obtain localized solutions, it is necessary that $F < F_m < 1$ where F_m is that critical value for which the phase and group velocities coincide at a finite non-zero wavenumber (a formal definition is given in Chapter 2). The validity of the linearized theory then requires that not only should the forcing be sufficiently small ($\epsilon \ll 1$), but also that F be bounded away from F_m. When this criteria fail, a weakly nonlinear theory can be constructed which leads to a forced nonlinear Schrödinger equation (fNLS).

When $\tau < 1/3$, the problem is more complicated than the case $\tau > 1/3$. Now small-amplitude solutions take the form of envelope solitary waves, that is localized wave packets, and the relevant wekly nonlinear model is the fNLS equation (see Akylas (1993) for the case of zero surface tension, $\tau = 0$).

Unforced wave packet structures have attracted much attention over the past three decades. Zakharov (1968) showed that the two-dimensional evolution of water waves in deep water can be described by the nonlinear Schrödinger equation (NLS). Later Hasimoto and Ono (1972) derived this equation to study the stability of two-dimensional gravity waves in water of finite depth. This was then generalized to three-dimensional waves by Davey and Stewartson (1974). Kawahara (1975) included

the effects of surface tension for two-dimensional water waves, while the generalization to the three-dimensional case was done by Djordjevic and Redekopp (1977). In this thesis, we extend the NLS equation obtained by Kawahara (1975) to the fNLS equation. Such details will be shown in Section 7.2. Also we will show that there is good agreement between the results from this fNLS model and our fully nonlinear results in Section 7.3.

7.1 Nonlinear Schrödinger Equation

In this Section, the weakly nonlinear theory for modulated gravity-capillary waves in water of finite depth is considered. First we consider unforced waves. Initially in this Section, we use the original dimensional coordinates for unsteady waves in standard notation in order that we can most easily make comparison with earlier works. In a frame of reference moving with the group velocity, $c_g = \partial\omega/\partial k$, we can write the solution for the free surface elevation η as

$$\eta = \mu A \exp i(kx - \omega t) + \text{c.c.} + \cdots . \tag{7.1}$$

Here A is the amplitude of a wave packet with oscillation wavenumber k and frequency ω satisfying the linear dispersion relation. We introduce $\xi = \mu(x - c_g t)$ and $T = \mu^2 t$ and let $A = A(\xi, T)$, where $c_g = d\omega/dk$ is the group velocity and $\mu << 1$. Then the envelope A is governed by the NLS equation (see Kawahara (1975) for the derivation)

$$iA_T + \lambda A_{\xi\xi} + \nu|A|^2 A = 0 \tag{7.2}$$

where

$$\begin{aligned} \lambda = \frac{1}{2}\frac{d^2\omega}{dk^2} &= -\frac{1}{8\omega^3}\{(g^2 - 6gTk^2 - 3T^2k^4)\sigma^2 - 2(g + Tk^2)(g + 3Tk^2)kh(\sigma - \sigma^3) \\ &+ (g + Tk^2)^2 k^2 h^2 (1 + 2\sigma^2 - 3\sigma^4)\} \end{aligned}$$

(7.3)

and

$$\begin{aligned}\nu &= -\frac{k^2}{4\omega\sigma}\Big[\frac{k}{\{g\sigma^2+Tk^2(\sigma^2-3)\}}\{g^2(9\sigma^4-10\sigma^2+9)+gTk^2(15\sigma^4-44\sigma^2+30)\\ &\qquad +T^2k^4(6\sigma^4-25\sigma^2+21)\}\\ &+ \frac{2(g+Tk^2)}{(\frac{d\omega}{dk})^2-gh}\{6(g+Tk^2)\sigma-2(g+3Tk^2)\sigma^3+3(g+Tk^2)kh(1-\sigma^2)^2\}\Big]\end{aligned} \tag{7.4}$$

where $\sigma = \tanh kh$. We also obtain the linear dispersion relation

$$\omega^2 = gk(1+\tau k^2h^2)\tanh kh\,. \tag{7.5}$$

We seek a solution of (7.2) in the form of an envelope solitary wave, that is,

$$A(\xi,T) = R(\chi)\exp i(\kappa\xi-\sigma T) \tag{7.6}$$

where $\chi = \xi - VT$ is a moving frame with respect to the frame (ξ,T), and V and κ are constants. Substituting equation (7.6) in the NLS equation (7.2) leads to an ordinary differential equation for $R(\xi)$,

$$\lambda\frac{d^2R}{d\chi^2}+(\sigma-\lambda\kappa^2)R+\nu R^3=0 \quad \text{with} \quad V=2\kappa\lambda. \tag{7.7}$$

Imposing the condition that $R(\chi)$ and $dR(\chi)/d\chi \to 0$ for $\chi \to \pm\infty$, the following result is obtained

$$R = a\,\mathrm{sech}\gamma\xi\,, \quad \text{with} \quad \gamma^2=\frac{\nu a^2}{2\lambda}\,,\ \sigma=\lambda(\kappa^2-\gamma^2)\,. \tag{7.8}$$

Here κ and the amplitude a are two free parameters. Note that this solution is valid only under the condition that $\nu\lambda > 0$.

Next, we consider the higher-order NLS equation given by

$$iA_T+\lambda A_{\xi\xi}+\nu|A|^2A+i\mu\{\lambda_1A_{\xi\xi\xi}+\nu_1|A|^2A_\xi+\nu_2A^2A^*_\xi\}=0\,. \tag{7.9}$$

Here

$$\lambda_1 = -\frac{1}{6}\frac{\partial^3 \omega}{\partial k^3}$$

while the higher-order nonlinear coefficients ν_1, ν_2 can be expressed as derivatives with respect to k of the nonlinear coefficient ν, but it will turn out that their exact values are not needed here. An envelope solitary wave is now given by

$$A = \{R(\chi) + i\mu R_1(\chi)\} \exp i(\kappa\xi - \sigma T)\,. \tag{7.10}$$

Without any loss of generality, we can assume that both R, R_1 are real-valued, as any imaginary part to R_1 can be absorbed into R. Substitution into equation (7.9) now yields

$$(\lambda - 3\mu\lambda_1\kappa)R_{\chi\chi} + (\sigma - \lambda\kappa^2 + \mu\lambda_1\kappa^3)R + (\nu - \mu(\nu_1 - \nu_2)\kappa)R^3 + \mu(V - 2\kappa\lambda)R_{1\chi} = 0\,, \tag{7.11}$$

$$\mu\{\lambda R_{1\chi\chi} + (\sigma - \lambda\kappa^2)R_1 + \nu R^2 R_1\} + \mu F_1 = 0 \tag{7.12}$$

$$\text{where} \quad F_1 = \lambda_1 R_{\chi\chi\chi} - (V_1 + 3\lambda_1\kappa^2)R_\chi + (\nu_1 + \nu_2)R^2 R_\chi\,. \tag{7.13}$$

Here we have expanded $V = 2\kappa\lambda + \mu V_1$. At leading order in μ, we obtain the previous result that R, V are given by (7.7) and (7.8). Next, we see that equation (7.11) for R is identical in form to equation (7.7) and so has the same solution (7.8) with modified coefficients. Next equation (7.12) for R_1 reduces to

$$\mu\{\lambda R_{1\chi\chi} + (\sigma - \lambda\kappa^2)R_1 + \nu R^2 R_1\} + \mu F_1 = 0\,. \tag{7.14}$$

This inhomogeneous equation for R_1 needs a compatibility condition, that is F_1 should be orthogonal to R which is the bounded solution of the homogeneous equation for R_1 (that is, (7.12) with $F_1 = 0$). Thus we require that

$$\int_{-\infty}^{\infty} R F_1 d\chi = 0\,. \tag{7.15}$$

But from (7.13), this is automatically satisfied and imposes no constraint on R_1. But if we look further into equation (7.12), we see that as $\chi \to \pm\infty$ F_1 has a leading order term proportional to $\exp(\mp\gamma\chi)$. Since the bounded solution to the homogeneous equation for R_1 is just R it will have the same behaviour. Hence the inhomogeneous equation will have solutions behaving like $\chi\exp(\mp\gamma\chi)$ as $\chi \to \pm\infty$, which is unacceptable. To avoid this we must put to zero the coefficient of $\exp(\mp\gamma\chi)$ in F_1 as $\chi \to \pm\infty$, which gives

$$V_1 = -3\lambda_1\kappa^2 \quad \text{so that} \quad V = 2\kappa\lambda - \mu 3\lambda_1\kappa^2\,. \tag{7.16}$$

It now follows from (7.1) and (7.10) that the crests within the packet (7.1) move with the phase speed

$$c = \frac{\omega(k) + \mu\kappa c_g(k) + \mu^2\sigma}{k + \mu\kappa}\,, \tag{7.17}$$

$$\text{or} \quad c = \frac{\omega(k+\mu\kappa)}{k+\mu\kappa} - \frac{\mu^2\nu a^2}{2k} + O(\mu^3)\,. \tag{7.18}$$

That is the linear phase speed $c_p(k+\mu\kappa)$ slightly modified by finite amplitude effects. The envelope speed is

$$c_g(k) + \mu V = c_g(k+\mu\kappa) + O(\mu^3) \tag{7.19}$$

after using (7.8) and (7.16) which is just the linear group velocity to leading order. Since these are not equal in general, the envelope solution defined by (7.1) is not a true solitary wave of the full equations.

But now, following the argument of Akylas (1993) for the case $\tau = 0$, suppose that the linear phase speed has a local extremum at a particular value of the oscillation wave number $k = k_m$. Then the linear group velocity $c_g(k_m)$ is equal to the linear phase speed $c_p(k_m)$. It follows that the bifurcation condition for a small-amplitude envelope solitary wave can be found by equating (7.18) with (7.19) upon putting

$k + \mu\kappa = k_m + \mu^2\Delta$ (that is, in effect $k = k_m$ and $\kappa = \mu\Delta$). This gives

$$\Delta = -\frac{\nu}{\lambda}\frac{a^2}{4k_m}. \tag{7.20}$$

Since here we can show that $\lambda(k = k_m) > 0$, and $\nu(k = k_m) > 0$ for gravity-capillary wave problem, we satisfy the condition that $\lambda\nu > 0$. Also then $\Delta < 0$ (that is, $k < k_m$) and so $c < c_p(k_m)$ as required.

7.2 Forced Nonlinear Schrödinger Equation

The derivation now follows the same path as above for the unforced NLS, but with a small extra forcing term (see Akylas (1993) for the case when there is no surface tension, and Părău and Dias (2000) for a different approach using normal form theory in the present case). To find the appropriate forcing term, it is sufficient to consider just the linear problem, which is,

$$\eta_t + U\eta_x = \phi_y, \quad \phi_t + U\phi_x + g(\eta - \tau h^2\eta_{xx}) = -\epsilon p(x) \quad \text{at} \quad y = 0\,, \tag{7.21}$$

together with Laplaces equation for ϕ in $-h < y < 0$ and $\phi_y = 0$ at $y = -h$. This is just the unsteady version of the linearized problem for perturbations to a uniform stream discussed in Chapter 2, now in dimensional form. Next, as in Chapter 2, the Fourier transform in x of η is

$$\eta' = \int_{-\infty}^{\infty} \eta \exp(-ikx)dx\,. \tag{7.22}$$

Taking the Fourier transform in x to (7.21), this gives

$$\eta'_t + ikU\eta' \;=\; \phi'_y, \tag{7.22a}$$

$$\text{and} \quad \phi'_t + ikU\phi' + g\eta' = -\epsilon p'\,, \tag{7.22b}$$

where $\phi' = C(k,t)\cosh k(y+h)$. Then solving (7.22a,b) for $C(k,t)$, yields

$$C = \frac{\eta'_t + ikU\eta'}{k \sinh kh} .$$

Rewritting (7.22a), now gives

$$\{\frac{\partial}{\partial t} + iUk\}^2\eta' + \omega^2(k)\eta' = -k \tanh kh \ \epsilon p' . \tag{7.23}$$

This is easily solved, but here we are concerned only with the case when $U = U_m + \mu^2\delta$ where $U_m = c_m = \omega(k_m)/k_m$ being the minimum phase speed and occurs for a wavenumber k_m as before. Hence we look for a solution in which

$$\eta = \mu A(X,T) \exp(ik_m x) , \tag{7.24}$$

where $X = \mu x, T = \mu^2 t$. Note that for a truly steady solution, A would not depend on T but it is useful to retain this for now. Then, using (7.22) we get

$$\eta' = A'(\kappa, T) = \int_{-\infty}^{\infty} A(X,T) \exp(-i\kappa X) dX , \tag{7.25}$$

where $k - k_m = \mu\kappa$. Substitution into (7.23) then gives at leading order

$$iA'_T - k_m\delta A' + \lambda\kappa^2 A' = -\frac{\epsilon\omega_m}{2g^*\mu^2} p\prime , \tag{7.26}$$

where $g^* = g(1 + \tau h^2 k_m^2)$ and λ is given by (7.3) evaluated at $k = k_m$. Then, inverting the Fourier transform (7.26) we get

$$-iA_T + k_m\delta A + \lambda A_{XX} = \frac{\epsilon\omega_m}{2g^*\mu^3} p \exp(-ik_m x) . \tag{7.27}$$

But here $p = p(X/\mu)$ and in the limit $\mu \to 0$ this is replaced by the δ-function, $\mu p_m \delta(X)$ where

$$p_m = \int_{-\infty}^{\infty} p(x) \exp(-ik_m x) dx$$

is the Fourier transform of $p(x)$ at $k = k_m$. Clearly we must choose $\epsilon = \mu^2$. So now we have

$$-iA_T + k_m\delta A + \lambda A_{XX} = \frac{\omega_m p_m}{2g^*} \delta(X) . \tag{7.28}$$

The right-hand side provides the connection between the pressure forcing in the full problem, and the forcing term in the forced NLS equation. In practice, as discussed below, we replace the δ-function with a smooth localized function whose area is unity. Finally we include the nonlinear term

$$-iA_T + k_m\delta A + \lambda A_{XX} + \nu|A|^2A = \frac{\omega_m p_m}{2g^*}\delta(X) \tag{7.29}$$

where ν is the same as in the unforced equation (7.2) but evaluated at $k = k_m$. Note that the sign difference in the term A_T compared to (7.2) which is due to the different reference frame here.

We now seek a solution of (7.29) in the form of a steady envelope solitary wave, that is, $A = A(X)$ where we may take A as real-valued since when the forcing function is symmetric in X, then the Fourier transform p_m is real-valued. At the same time the equation is written in terms of the original unscaled variables. Thus (7.24) is replaced by

$$\eta \;=\; A(x)\exp\left(ik_m x\right) + \text{c.c.}\,, \tag{7.30}$$

$$\text{and} \qquad \Delta k_m A + \lambda A_{xx} + \nu|A|^2A \;=\; \frac{\omega_m \epsilon p_m}{2g^*}\delta(x)\,. \tag{7.31}$$

where $\Delta = U - U_m$. This is an ordinary differential equation in $A(x)$, whose symmetric solutions for $x > (<)0$ are

$$A = a\,\text{sech}\gamma(x \mp x_0)\,, \quad \text{with} \quad \gamma^2 = \frac{\nu a^2}{2\lambda}\,,\; k_m\Delta = -\lambda\gamma^2\,. \tag{7.32}$$

Next we must use the jump condition at $x = 0$, obtained by integrating (7.31) across a small interval about the origin,

$$\lambda[A_x]_{0-}^{0+} = \frac{\omega_m \epsilon p_m}{2g^*}\,. \tag{7.33}$$

Hence we get

$$2\lambda\gamma a\,\text{sech}\gamma x_0 \tanh\gamma x_0 = \frac{\omega_m \epsilon p_m}{2g^*}\,. \tag{7.34}$$

This determines x_0 in terms of p_m and a and so completes the solution. The Froude number is $F = U/\sqrt{gh}$ and so for a given F, we have Δ, hence a, γ from (7.32) and finally x_0 from (7.34). Note that the central amplitude is $a_m = a\,\mathrm{sech}\gamma x_0$. To obtain the bifurcation curve, we rewrite (7.34) as

$$\{\frac{\omega_m \epsilon p_m}{2g^*}\}^2 = -4\lambda a_m^2 \{k_m \Delta + \frac{\nu a_m^2}{2}\}\,. \tag{7.35}$$

Thus the bifurcation curve is the same for $\epsilon > 0$ or < 0 and $a_m > 0$ or < 0. That is, the branch contains four solutions; one pair ($\epsilon > 0$) has a monotonic profile in $x > 0$ if $a_m < 0$ but is dimpled if $a_m > 0$, while the other pair ($\epsilon < 0$) has a monotonic profile in $x > 0$ if $a_m > 0$ but is dimpled if $a_m < 0$. But note that as in the forced Korteweg-de Vries model discussed in Chapter 6 for $\tau > 1/3$ case, not all branches are found. Here we must have $0 < \nu a_m^2/2 < -k_m\Delta$ (see (7.32)) and so the branches which lie outside the unforced solitary wave branch (that is, the case $\epsilon = 0$ so that $\nu a_m^2/2 = -k_m\Delta$) are not present. Also, there is no counterpart here of the "singular" solution of the forced Korteweg-de Vries model which remedied the corresponding defect there.

To find any missing branches the δ-function forcing must be replaced with a smooth forcing term. Suppose them, for instance, that we replace the δ-function in (7.31) with

$$K\mathrm{sech}(\gamma x)\,, \tag{7.36}$$

where K is chosen to make the integral of (7.36) equal to unity. In this case we seek a solution of the form

$$A = a\,\mathrm{sech}(\gamma x)\,. \tag{7.37}$$

but now we find that

$$\gamma^2 = \frac{\nu a^2}{2\lambda}\,, \qquad \text{and} \qquad a\{k_m\Delta + \frac{\nu a^2}{2}\} = \frac{K\omega_m \epsilon p_m}{2g^*}\,. \tag{7.38}$$

Note that now $a > 0 (< 0)$ and $\epsilon p_m > 0 (< 0)$ gives $k_m\Delta + \nu a^2/2 > 0$. Thus the "missing" branches are found. Conversely, the previous branches with $k_m\Delta + \nu a^2/2 < 0$ now require that $a > 0 (< 0)$ as $\epsilon p_m < 0 (> 0)$ and so the previous "dimpled" solutions are not found here. If they do exist for the fNLS equation with the forcing term (7.36) numerical integration is needed, but see below in next Section for more comment on this issue. Further, this solution is anomalous in that the above branch extends to the forbidden region $\Delta > 0$. The reason is that here the forcing (7.36) extends to infinity, unlike the δ-function forcing in (7.31), and the solution (7.37) has the same decay rate at infinity as the forcing. Hence the usual argument about why $\Delta < 0$ does not apply.

This suggests that (7.36) is not a good choice as a forcing term, and a better one is

$$K\mathrm{sech}^3(\gamma x)\,. \tag{7.39}$$

Here, K is chosen so that the area under the forcing function is again unity. In this case again we seek a solution

$$A = a\mathrm{sech}(\gamma x)\,. \tag{7.40}$$

Now the forcing (7.39) decays more rapidly at infinity than the solution (7.40). We find that

$$k_m\Delta = -\lambda\gamma^2 \qquad \text{and} \qquad a\{k_m\Delta + \frac{\nu a^2}{2}\} = \frac{K\omega_m\epsilon p_m}{2g^*}\,. \tag{7.41}$$

Note that (7.41) is in fact identical to (7.38) but now $\Delta < 0$ is required. But again the "dimpled" solutions are not found, and presumably again need numerical integration. Also, the expression (7.41) includes the branch with $a > 0$ which (7.38) does not allow.

7.3 Comparison of fNLS and Nonlinear Results

To make a connection with the nonlinear numerical results, in this Section we choose the pressure distribution $U^2 p(x)/2$ to be the same as that used in the numerical results, but reduced for the present weakly nonlinear limit. That is, we let

$$p(x) = \exp[\frac{{x_b}^2}{x^2 - {x_b}^2}] \quad \text{for} \quad |x| < x_b \,, \tag{7.42}$$

and zero elsewhere. As above the δ-function in (7.31) is then replaced by a smooth function such that the area under the curve of this function is unity. Thus we make the substitution

$$\delta(x) \to \frac{p(x)}{p_0} \quad \text{where} \quad p_0 = \int_{-\infty}^{\infty} p(x)\, dx \,.$$

Then equation (7.31) becomes, in dimensionless coordinates based on length scale H and velocity scale $(gH)^{1/2}$,

$$(F - F_m)k_m A + \lambda_m A_{xx} + \nu_m |A|^2 A \;=\; \frac{F^2 \epsilon\, \omega_m\, p_m}{4p_0(1 + \tau k_m^2)} p(x) \,. \tag{7.43}$$

Strictly speaking $F = F_m$ on the right-hand side, but we will retain F in the above equation. Here λ_m, ν_m are the nondimensional values of λ, ν at $k = k_m$.

We will find $A(x)$ numerically by using a high-order Runge-Kutta method. To do this numerically, we set initial conditions at $x = L$ where $L \gg x_b$. That is, we put

$$A(x) = a_0 \exp(-2\gamma L) \,, \quad A_x = -2\gamma a_0 \exp(-2\gamma L) \,,$$
$$\text{where} \quad \gamma^2 = -\frac{k_m(F - F_m)}{\lambda} \,.$$

We assume that A is real, and then integrate from L to 0. Then a_0 is varied until $\eta_x(x = 0) = 0$ is satisfied. Note that we need to find both elevation and depression waves, and presumably these have $a_0 > 0$ and $a_0 < 0$ respectively. Also, for this fNLS the change $\epsilon \to -\epsilon$ and $A \to -A$ leaves the equation unchanged. This implies

that all solutions for $\epsilon < 0$ can be found as mirror images of those for $\epsilon > 0$. Thus, it is sufficient to solve for $\epsilon > 0$ and find both depression and elevation waves, since the branches for $\epsilon < 0$ are simply found by changing $A(0)$ to $-A(0)$ as above. Also since two branches have a turning point, there can be two solutions for a given F implying that for a fixed $\epsilon > 0 (\text{or} < 0)$ there are potentially three solutions. Finally, the free surface profiles are obtained from (7.30),

$$\eta = 2\,A(x)\,\cos\left(k_m x\right).$$

The values of ν and λ in the fNLS equation are scaled by using $\sqrt{gH}$ as a unit velocity and H as a unit length. When $\tau = 0.25$, the corresponding critical values are as follows : $k_m = 1.402$, $\omega_m = 1.361$, $F_m = 0.9707$, $\lambda_m = 0.045$, $\nu_m = 119.9$, $p_m = 0.4562$ and $p_0 = 0.6438$. Note that $\lambda_m \nu_m > 0$ for this value of τ as required. Indeed it can be shown that $\lambda_m \nu_m > 0$ for all τ, $0 < \tau < 1/3$.

Depression waves

For small ϵ, the fNLS model predicts the existence of all branches found numerically. The branches for $\epsilon = 0.001,\ 0$ and -0.001 for depression waves are shown in Figure 7.1 (those for elevation waves are mirror images of these with the sign of ϵ reversed as discussed above). These branches correspond to the fully nonlinear results shown in Figures 5.1. Interestingly while we see good qualitative agreement, the quantitative agreement is markedly better for depression waves than for elevation waves. Figure 7.2 shows the free surface profile $\eta(x)$ and the envelope $A(x)$ obtained from integrating the fNLS equation (7.43). From Figure 7.1 we see that the $\epsilon < 0$ branch crosses the unforced ($\epsilon = 0$) branch, and a "dimpled" solution exists above this unforced branch. This behavior agrees qualitatively with the analysis in Section 7.2 with the δ-forcing (compare also the results presented by Părău and Dias (2000)). However, when we use the actual forcing, we see that the branch with negative forcing does exist, but lies below the unforced branch until the dimple appears, after which it lies above the unforced branch. In contrast, using the δ-function forcing places the "dimpled" branch always above the unforced branch, and in fact coincident with the "monotonic" branch.

Next we compare the depression wave solutions of the fNLS equation (7.43) with the numerical solutions of the fully nonlinear equations, and also with the linear solutions. For $\epsilon = 0.0001$, the relationship between $\eta(0)$ and F of the linear, fNLS and nonlinear solutions are shown in Figure 7.3. As expected, the numerical solutions of (7.43) confirm the previous analysis corresponding to the bifurcation curve (7.41). Two solutions are found at the same value of F. That is, one solution (the upper curve) is the bifurcation from a uniform stream and the other (the lower curve) is the bifurcation from an envelope solitary wave. From Figure 7.3, results from the fNLS model agree well with the fully nonlinear results along the upper curve and as

F nears F_m. But unlike the fNLS solutions, the linear solutions for $\epsilon > 0$ are in good agreement with fNLS and nonlinear solutions only when F is not too close to F_m. Along the lower curve, we find that the differences in amplitude between the fNLS and nonlinear results emerge as F decreases away from F_m since the wave amplitude increases as F decreases. This behaviour of the fNLS solutions are consistent with the assumptions made in the derivation of the fNLS model. The comparison of the computed free surface profiles between fNLS and nonlinear results are shown in Figures 7.6-7.8. The comparison for $\epsilon = 0.0001$ and on the lower branch is shown in Figure 7.6. Although there is a difference in the amplitudes, the wavelength calculated from the two approaches is in good agreement with the predicted value $2\pi/k_m$.

A comparison of the depression solitary waves for $\epsilon = 0$ obtained from the NLS model and the fully nonlinear numerical solution are shown in Figure 7.4, and a typical free surface profile is shown in Figure 7.7. It is clear from these results that bifurcation occurs at the critical value F_m as expected (compare Buffoni, Champneys and Toland (1996)), even although we are unable to obtain accurate nonlinear solutions as F approaches F_m due to inflexion points on the wave profile. Finally there also exist depression wave solutions in the case of $\epsilon < 0$, shown in Figure 7.5 and Figure 7.8. Again, results from fNLS and nonlinear problems are in good agreement when the wave amplitude is relatively small.

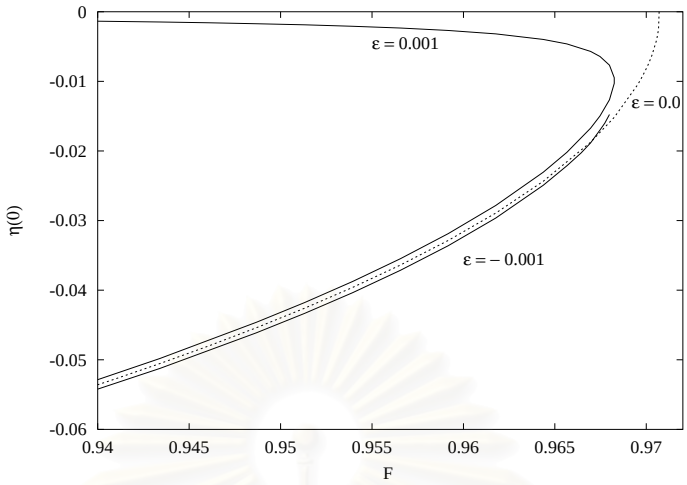

Figure 7.1: Relationship between F and $\eta(0)$ from fNLS results

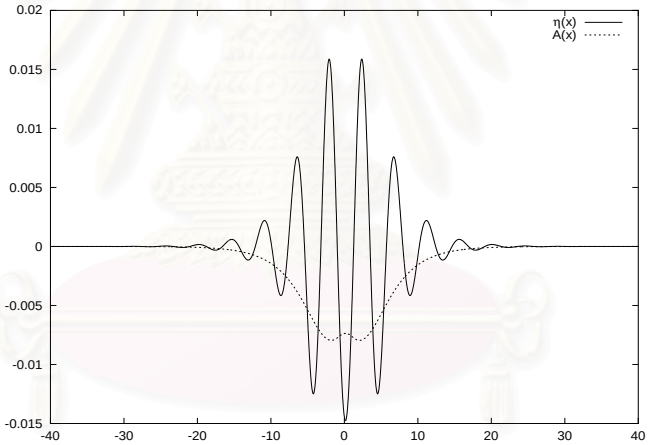

Figure 7.2: Free surface profile from the fNLS when $F = 0.968$ and $\epsilon = -0.001$

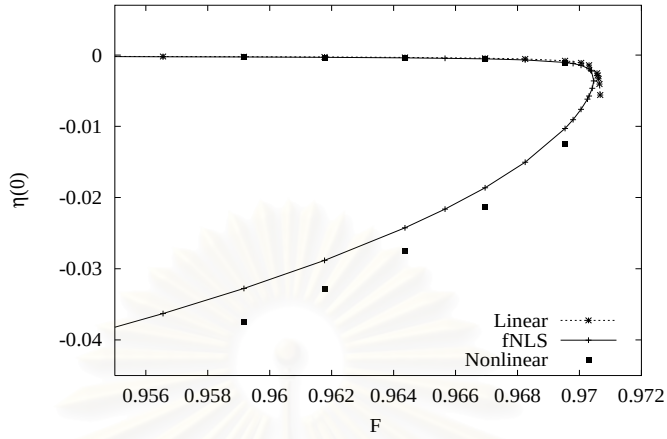

Figure 7.3: Relationship between F and $\eta(0)$ when $\tau = 0.25$ and $\epsilon = 0.0001$

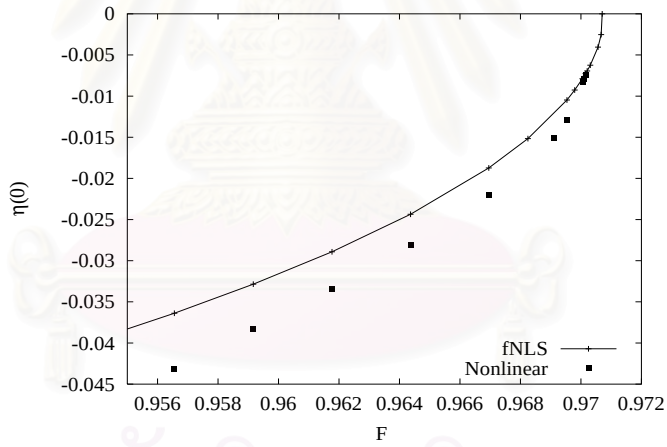

Figure 7.4: Relationship between F and $\eta(0)$ when $\tau = 0.25$ and $\epsilon = 0.0$

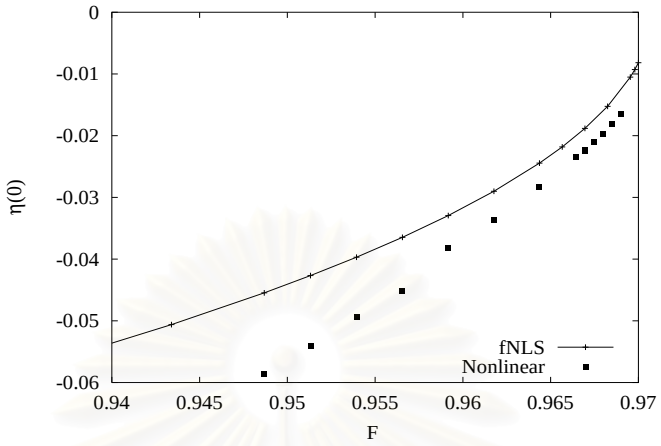

Figure 7.5: Relationship between F and $\eta(0)$ when $\tau = 0.25$ and $\epsilon = -0.0001$

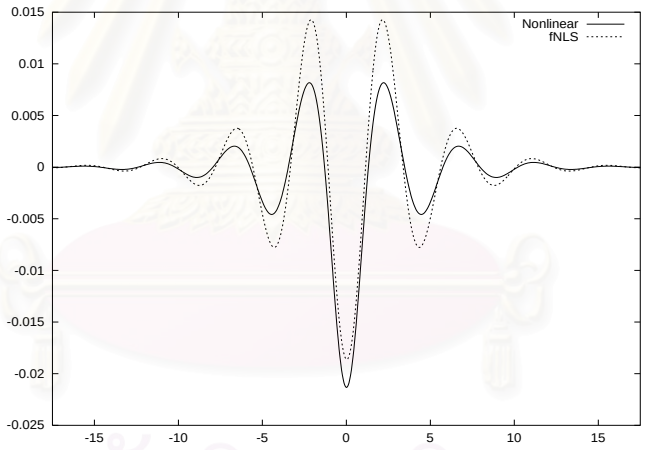

Figure 7.6: Comparison of free surface profiles when $F = 0.96695$ and $\epsilon = 0.0001$

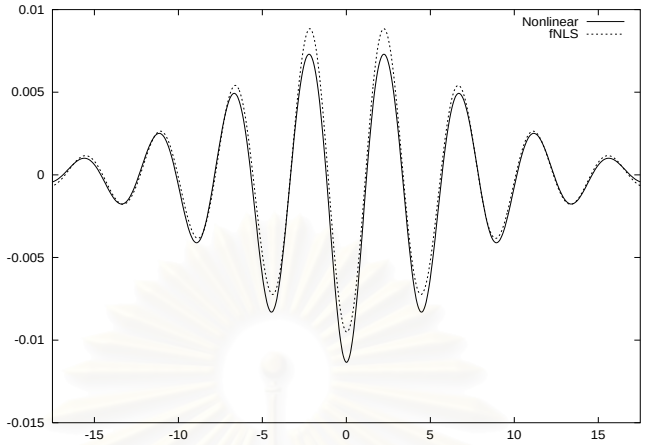

Figure 7.7: Comparison of free surface profiles when $F = 0.96974$ $\epsilon = 0.0$

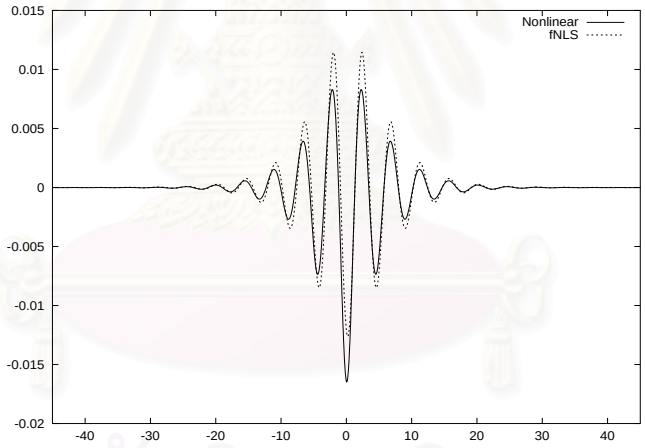

Figure 7.8: Comparison of free surface profiles when $F = 0.96902$ and $\epsilon = -0.0001$

Elevation waves

For $\tau < 1/3$, we have found that elevation waves exist for both $\epsilon > 0$ and < 0 as predicted by the fNLS model. This is different from the case of $\tau > 1/3$ when solutions can only be found when $\epsilon < 0$. For $\epsilon < 0$ and $\tau < 1/3$, the branches of elevation waves from the linear theory, the fNLS model and the fully nonlinear results are shown in Figure 7.9. There are two types of solutions, one (the lower curve) is a perturbation from a uniform stream, and the other (the upper curve) is a perturbation from an envelope solitary wave. The fNLS results agree well with the nonlinear results when the wave is of small amplitude and F is close to F_m, while linear results give better prediction to the perturbed solutions from the uniform stream. The corresponding comparison of the computed free surface profiles on the upper curve for $\epsilon = -0.0001$ is shown in Figure 7.12.

It should be noted that fNLS is not a good model equation to described wave solutions when $|F - F_m|$ is sufficiently large. In that case the nonlinear solution is a better choice to gain insight into the solution behaviours. Figure 7.10 and Figure 7.13 give a comparison of elevation solitary waves ($\epsilon = 0$) obtained from the NLS model with the fully nonlinear results. These again show that elevation solitary wave solutions bifurcate from the critical value F_m, just as for depression waves. But we recall here that the NLS and fNLS model predicts complete symmetry between depression and elevation waves. However, although this does occur in the limit as the wave amplitude decreases and $F \to F_m$ it is apparent from a comparison of Figure 5.1 and Figure 5.8 that this is not so for the fully nonlinear problem, where marked differences emerge as F decreases.

Finally in Figure 7.11 and Figure 7.14 we show the comparisons for elevation waves with $\epsilon > 0$. Note that the free surface profile obtained from the fNLS shown in Figure 7.14 corresponds to a "dimpled" envelope solution of the fNLS equation with

$A(x) > 0$. Again the qualitative agreement with the fNLS model is evident.

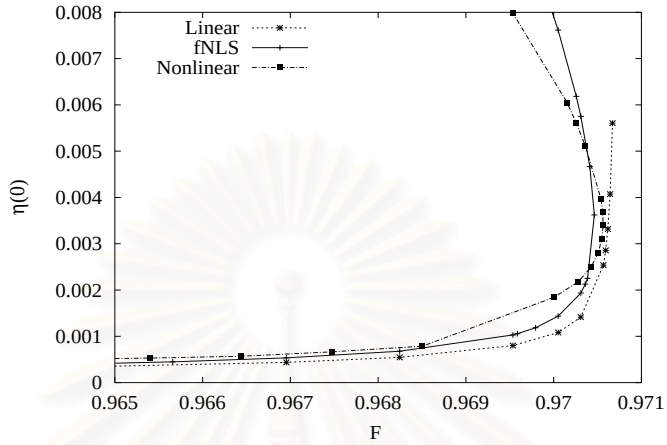

Figure 7.9: Relationship between F and $\eta(0)$ when $\tau = 0.25$ and $\epsilon = -0.0001$

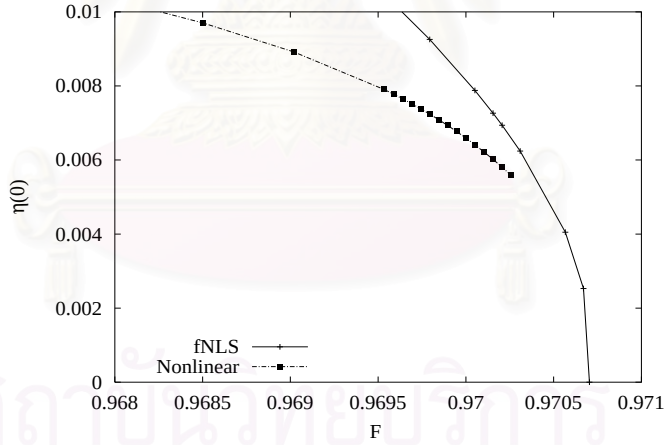

Figure 7.10: Relationship between F and $\eta(0)$ when $\tau = 0.25$ and $\epsilon = 0.0$

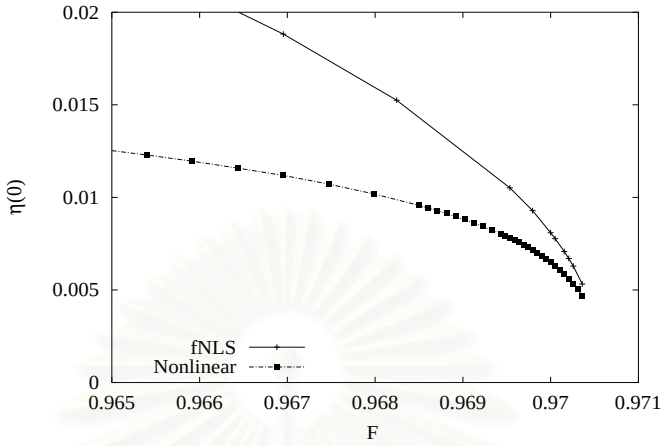

Figure 7.11: Relationship between F and $\eta(0)$ when $\tau = 0.25$ and $\epsilon = 0.0001$

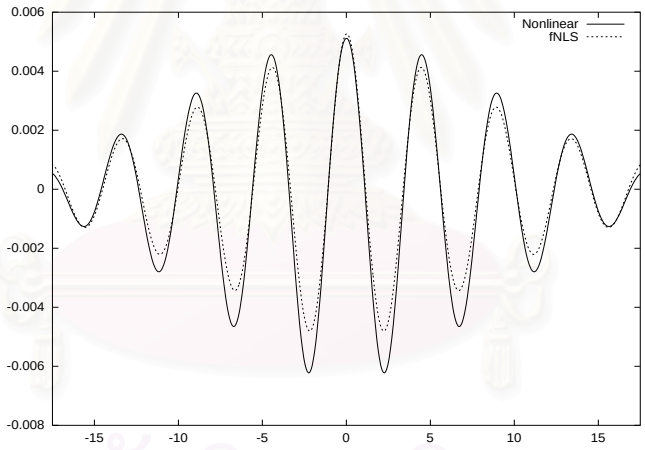

Figure 7.12: Comparison of free surface profiles when $F = 0.97036$ and $\epsilon = -0.0001$

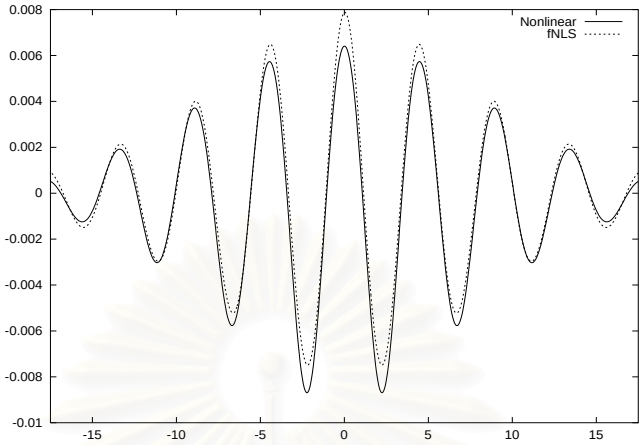

Figure 7.13: Comparison of free surface profiles when $F = 0.97005$ $\epsilon = 0.0$

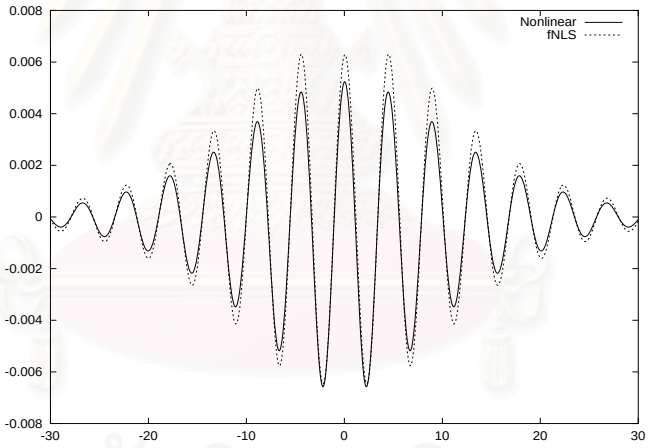

Figure 7.14: Comparison of free surface profiles when $F = 0.97026$ and $\epsilon = 0.0001$

CHAPTER VIII

CONCLUSION

In this thesis we have presented some numerical results for the calculation of symmetric steady subcritical free surface flows due to an applied localized pressure distribution. Both gravity and surface tension effects are taken into account. In the context of water wave problem, the value of the coefficient of surface tension, T, is 0.0736 N/m at 20^0C which corresponds to the total depth of water in the rest state about 0.48 cm when the value of Bond number is $1/3$. In our work, we have considered the case of surface-tension dominated waves when the Bond number $\tau > 1/3$. Of course, it has to be said that this case has very limited application, since it applies for such shallow water depths that it is unrealistic to neglect dissipation, as we have done here. Nevertheless, we feel that it is useful to expand the known results for unforced solitary waves to a context of forced waves in this particular problem where numerical results for finite-amplitude waves can be obtained, in order to increase our understanding of nonlinear waves in general.

Our numerical results show that both depression and elevation localized forced waves exist when $\tau > 1/3$. It is found that depression waves exist for both positive ($\epsilon > 0$) and negative forcing ($\epsilon < 0$). For $\epsilon > 0$, the solution branch which plots wave amplitude versus the Froude number F is multivalued. There are two depression waves for the same value of Froude number $F < 1$. One wave is a perturbation from the uniform flow and the other is a perturbation of a depression solitary wave. When $\epsilon < 0$, we found only one branch, which is a perturbation of the depression solitary

wave. As F decreases towards zero, both of these wave branches exhibit the same limiting configuration with a trapped bubble. For elevation waves, we found that this type of wave occurs only as a bifurcation from the uniform flow and exists only when $\epsilon < 0$.

To obtain insight into our numerical results when $\tau > 1/3$ we considered both the linearized theory and a weakly nonlinear theory leading to the forced KdV equation. In the case of elevation waves, both the linearized theory and the results from the forced KdV model gave good agreement with nonlinear results for relatively small $\epsilon = -0.001$. As F approaches 1 and ϵ is larger ($\epsilon = -0.1$), the linear theory fails. But for this value of ϵ the forced KdV model remains a good predictor, although it begins to fail when ϵ is increased further. In the case of depression waves, for ϵ is small, the bifurcation diagram from the weakly nonlinear analysis of the forced KdV model closely fits the numerical results. On the upper part of this branch, the linearized theory can also predict the perturbation from the uniform flow, provided that F is not too close to 1. Further the forced KdV model can also predict the depression wave when $\epsilon = -0.001 < 0$.

We have also considered the case of gravity-dominated waves when the Bond number, $\tau < 1/3$. This case is more complicated than the previous case. We found that the finite-amplitude wave solution for both depression and elevation waves exist. Also, we expect these results to persist in qualitative form as τ is decreased, although the numerical calculations become extremely lengthy when τ is small.

Our numerical results when $\tau < 1/3$ show that both depression and elevation localized forced waves exist. It is found that depression and elevation waves exist for both positive($\epsilon > 0$) and negative forcing($\epsilon < 0$). The solution branches which plot wave amplitude versus the Froude number F is multivalued for depression waves when $\epsilon > 0$ and for elevation waves when $\epsilon < 0$. One solution is a perturbation

from the uniform flow and the other is a perturbation of a solitary wave. We found only one branch, which is a perturbation of the solitary wave, for depression waves when $\epsilon < 0$ and for elevation waves when $\epsilon > 0$. In the case of depression waves, as F decreases, both of these wave branches exhibit a limiting configuration with a trapped bubble which can occur only when $\tau < 1/2$, whereas a limiting configuration with flow due to a sink can be found when $\tau > 1/2$.

To gain insight into our numerical results when $\tau < 1/3$, we considered both the linearized theory and a weakly nonlinear theory leading to the forced nonlinear Schrödinger (fNLS) equation. In the case of depression waves, for ϵ is small and positive, the bifurcation diagram from the weakly nonlinear analysis of the fNLS model closely fits the numerical results, indicating that the forced solutions are bifurcations from an envelope solitary wave. On the upper part of this branch, the linearized theory can also predict the bifurcation from the uniform flow state, provided that F is not too close to F_m. The fNLS model can also predict the depression wave when $\epsilon = -0.0001 < 0$. Similar conclusions can be made for elevation waves as then the fNLS model predicts the same behaviour but for the opposite sign of ϵ. But in this case for the fully nonlinear results, while agreeing as expected as the wave amplitude decreases and $F \to F_m$, significant differences emerge as F decreases. Our numerical results show that as F decreases, the number of inflexion points on the free surface decrease, while the wave amplitude increases to a maximum value and then decreases again. The fNLS model cannot predict this behaviour.

Also, some wave solutions in the form of multi-hump solutions were obtained in our numerical calculations. We have presented some typical behaviour as the flow parameters are varied. Further study is needed to understand these solutions and any connection with weakly nonlinear models.

REFERENCES

Akylas, T. R. On the excitation of long nonlinear water waves by a moving pressure distribution. *J. Fluid Mech.* 141(1984): 455-466.

Akylas, T. R. Envelope solitons with stationary crests. *Phys. Fluids.* A5(1993): 789-791.

Amick, C.J.; and Kirchgässner, K. A theory of solitary waves in the presence of surface tension. *Arch. Rational Mech. Anal.* 105(1989): 1-49.

Asavanant, J.; and Vanden-Broeck, J.-M. Free surface flows past a surface piercing object of finite length. *J. Fluid Mech.* 273(1994): 109-124.

Buffoni, B.; Champneys, A.R.; and Toland, J.F. Bifurcation and coalescence of a plethora of homoclinic orbits for a Hamiltonian system. *J. Dyn. Diffl. Equat.* 8(1996): 221-279.

Calvo, D.C.; and Akylas, T.R. Stability of steep gravity-capillary solitary waves in deep water. *J. Fluid Mech.* 452(2002): 123-143.

Davey, A.; and Stewartson, K. On three dimensional packets of surface waves. *Proc. R. Soc. Lond.* A338(1974): 101-110.

Dias, F.; and Iooss, G. Water waves as a spatial dynamical system. *Handbook of Mathematical Fluid Dynamics* 2, ed. Friedlander and Serre, Elsevier, (2003): 443-499.

Dias, F.; and Kharif, C. Nonlinear gravity and capillary-gravity waves. *Annu. Rev. Fluid Mech.* 31(1999): 301-346.

Dias, F.; Menasce, D.; and Vanden-Broeck, J.-M. Numerical study of capillary-gravity solitary waves. *Eur. J. Mech., B/Fluids.* 15(1996): 17-36.

Dias, F.; and Vanden-Broeck, J.-M. Steady two-layer flows over an obstacle. *Phil. Trans. Roy. Soc. London A.* 360(2002): 2137-2154.

Djordjevic, V. D.; and Redekopp, L.G. On two dimensional packets of capillary-gravity waves. *J. Fluid Mech.* 79(1977): 703-714.

Grimshaw, R. Nonlinear effects in wave scattering and generation. *Proceedings of the IUTAM Symposium on Diffraction and Scattering in Fluid Mechanics and Elasticity.* Manchester, I.D. Abrahams, P.A. Martin and M.J. Simon, Kluwer, Dordrecht (2000): 23-34.

Grimshaw, R.; and Iooss, G. Solitary waves of a coupled Korteweg-de Vries system. *Math. Comput. Simulation.* 64(2003): 31-40.

Hasimoto, H.; and Ono, H. Nonlinear modulation of gravity waves *J. Phys. Soc. Japan* 33(1972): 805-811.

Hunter, J.K.; and Vanden-Broeck, J.-M. Solitary and periodic gravity-capillary waves of finite amplitude. *J. Fluid Mech.* 134(1983): 205-219.

Iooss, G.; and Kirchgässner, K. Bifurcation d'ondes solitaires en présence d'une faible tension superficielle. *C.R. Acad. Sci. Paris, Série I.* 311(1990): 265-268.

Kawahara, T. Nonlinear self-modulation of capillary-gravity waves on liquid layer. *J. Phys. Soc. Japan.* 38(1975): 265-270.

Kirchgässner, K. Nonlinearly resonant surface waves and homoclinic bifurcation. *Adv. Appl. Mech.* 26(1988): 135-181.

Longuet-Higgins, M.S. Limiting forms of capillary-gravity waves. *J. Fluid Mech.* 194(1988): 351-375.

Părău, E.; and Dias, F. Ondes solitaires forcées de capillarité-gravité. *C. R. Acad. Sci. Paris.* t. 331, Série I (2000): 655-660.

Rayleigh, Lord. The form of standing waves on the surface of running water. *Proc. Lond. Math. Soc.* 15(1883): 69.

Schwartz, L.W. Nonlinear solutions for an applied over pressure on a moving stream. *J. Engrg. Math.* 12(1981): 147-156.

Vanden-Broeck, J.-M.; and Dias, F. Gravity-capillary solitary waves in water of infinite depth and related free surface flows. *J. Fluid Mech.* 240(1992): 549-557.

Zakharov, V.E. Stability of periodic waves of finite amplitude on the surface of a deep fluid. *J. Appl. Mech. Tech. Phys.* 2(1968): 190-194.

APPENDIX

APPENDIX

Monacella (1961) proved that a singularity in the Cauchy principal value integrals can be ignored in the numerical integration. This is achieved by spacing the mesh points symmetrically with respect to the pole. We show here by using the trapezoidal rule to compute the Cauchy principal value integral. We can also use the Simpson's rule to approximate such integral.

Let f be a continuous function. We approximate the integral of f over a finite interval $[a,b]$ by partitioning $[a,b]$ into N subintervals with $t_0 = a$ and $t_N = b$. Thus

$$\int_a^b f(t)dt \;\approx\; \sum_{i=0}^{N} f(t_i)W_i\,, \tag{1}$$

where

$$W_i = \begin{cases} \frac{h}{2},\ i = 0 \text{ and } N \\ \\ h,\ \text{otherwise.} \end{cases} \tag{2}$$

Here $h = (b-a)/N$. We consider a function $f(t)/(t-x)$ with $f(x) \neq 0$ and $x \in (a,b)$. The integral of $f(t)/(t-x)$ over the variable t is of Cauchy principal value form. For any $\epsilon > 0$, we can write this integral as

$$\int_a^b \frac{f(t)}{t-x}dt \;=\; \lim_{\epsilon\to 0}\Big[\int_a^{x-\epsilon}\frac{f(t)}{t-x}dt + \int_{x+\epsilon}^{b}\frac{f(t)}{t-x}dt\Big]. \tag{3}$$

To compute this integral, we rewrite the integral on the left hand side of (3) as

$$\int_a^b \frac{f(t)}{t-x}dt \;=\; \int_a^b \frac{f(t)-f(x)}{t-x}dt + f(x)\int_a^b \frac{1}{t-x}dt. \tag{4}$$

Next we consider $N+1$ equally spaced mesh point $t_i, i = 0, ..., N$ and let x is the midpoint between t_i and t_{i+1} for $i = 0, 1, ..., N-1$. There are two possible cases to be considered: (i) $x = (b+a)/2$ and (ii) $x \neq (b+a)/2$.

Case (i) $x = (b+a)/2$.

It can easily be shown that $\int_a^b \frac{dt}{t-x} = 0$. Thus (4) becomes

$$\int_a^b \frac{f(t)}{t-x}dt = \int_a^b \frac{f(t)-f(x)}{t-x}dt. \tag{5}$$

Using the trapezoidal rule, we approximate the integral on the right hand side of (5) by

$$\begin{aligned}\int_a^b \frac{f(t)}{t-x}dt &\approx \sum_{i=0}^{N} \frac{f(t_i)-f(x)}{t_i-x}W_i \\ &= \sum_{i=0}^{N} \frac{f(t_i)}{t_i-x}W_i - f(x)\sum_{i=0}^{N}\frac{W_i}{t_i-x} \\ &= \sum_{i=0}^{N} \frac{f(t_i)}{t_i-x}W_i. \end{aligned} \tag{6}$$

Here W_i and h are defined as in (2) and $\sum_{i=0}^{N} \frac{W_i}{t_i-x} = 0$ because x is the midpoint of the interval $[a, b]$. Equation (6) suggests that the Cauchy principle value integral can be approximated as if it were an ordinary integral.

Case (ii) $x \neq (b+a)/2$.

Assuming that x is a midpoint on any interval $[c, d] \subset [a, b]$. We now rewrite (3) as

$$\int_a^b \frac{f(t)}{t-x}dt = \int_a^c \frac{f(t)}{t-x}dt + \int_c^d \frac{f(t)}{t-x}dt + \int_d^b \frac{f(t)}{t-x}dt \tag{7}$$

The first and third integrals on the right hand side of (7) are not Cauchy principal values. Thus they can be approximated by the trapezoidal rule. The second integral is a Cauchy principle value with x as a midpoint of the interval $[c, d]$. The discussion

in case(i) shows that it can also be evaluated by the trapezoidal rule. Therefore

$$\int_a^b \frac{f(t)}{t-x}dt \approx \sum_{i=0}^{N} \frac{f(t_i)}{t_i - x} W_i$$

which is the same as (6). Thus, the singularity is subtraced from the Cauchy principal value integral leaving nonsingular integrals to be evaluated as claimed.

VITA

Mr.Montri Maleewong was born on January 21, 1975 in Bangkok. He received a Bachelor Degree in Mathematics in 1996 and a Master Degree in Computational Science in 1999 from the Department of Mathematics, Faculty of Science, Chulalongkorn University. His areas of research interest are Ground Water Modeling and Computational Fluid Dynamics related to the potential free surface flow problems.